Department of Mechanical Engineering
Solid Mechanics

ISRN LUTFD2/TFHF–06/5115–SE(1–81)

A SMALL DEFORMATION MODEL FOR THE ELASTO-PLASTIC BEHAVIOUR OF PAPER AND PAPERBOARD

Master's Thesis by

Tomas Andersson

Supervisors
Mikael Nygårds, STFI-Packforsk
Anders Harrysson, Div. of Solid Mechanics

Examiner
Mathias Wallin, Div. of Solid Mechanics

Printed by KFS i LUND AB, Lund, Sweden.

For information, address:
Division of Solid Mechanics, Lund University, Box 118, SE-221 00 Lund, Sweden.
Homepage: http://www.solid.lth.se

Acknowledgements

The master's thesis presented in this paper has been carried out in partial fulfilment of the degree Master of Science in Mechanical Engineering at Lund Institute of Technology. The work has been carried out at STFI-Packforsk in Stockholm, Sweden during the autumn of 2005, with supervision from the Division of Solid Mechanics at Lund Institute of Technology. Being part of the frontline of the paper research and development has gained me much knowledge and it has been a fun and interesting experience for me.

First of all I would like to express my gratitude to the initiator of the project, PhD Mikael Nygårds. As my supervisor at STFI-Packforsk he has put in much effort in order to help, inspire and support me throughout the project. I especially appreciate our discussions about paper mechanisms and model building, and for always being willing to read through my uncountable drafts. I would like to thank my supervisor at Lund Institute of Technology, PhD candidate Anders Harrysson, for his mindful explanations when answering my questions and for always getting me on the right track when answering my endless e-mails. I would like to show my appreciation to my examiner, PhD Mathias Wallin, for his interest in my work and I would especially like to thank him for the help on how to calculate the material stiffness tensor. Finally I would like to show my gratitude to Prof. Niels Saabye Ottosen for steering me onto the material modelling track in the first place.

A beautiful snow-white day in Lund, January 2006.

Tomas Andersson

Abstract

In order to optimize paper products and predict paper converting processes solid mechanics analyses can be conducted. In order to make accurate analyses reliable material models are required. In 2002 Q.S. Xia proposed a large deformation model for paperboard. The model consist of a continuum model that describes the behaviour of layers of fibres and an interface model that describes the delamination between layers of fibres. This master's thesis attempts to contribute to the further development of a reliable material model.

Three major aspects have been covered within this work. First, a small deformation continuum model for paper is proposed. Second, the proposed model is implemented into the commercial finite element program ABAQUS/Standard. Third, to illustrate the behaviour of the model, a simulation of creasing of paperboard is performed.

The continuum model consist of two parts which are solved separately; the in-plane model and the out-of-plane model. The in-plane model accounts for the behaviour of the two directions in the paper-plane and the shear between these two directions. The out-of-plane model controls the behaviour in the through-thickness direction of the paper and the shear between this direction and the two in-plane directions. The in-plane model proposed is a small deformation formulation of the model proposed by Xia (2002). In the original model by Xia (2002) the out-of-plane model does only has an elastic behaviour. The importance to have an elasto-plastic behaviour in these components has however been recognized and a model for this elasto-plastic behaviour have been developed. The behaviour of the normal component in the thickness direction is inspired by a model proposed by Stenberg (2003), treats the paper as a porous material and accounts for nonlinear elasticity that depends both on the elastic strain and the plastic strain. The out-of-plane shear behaviour proposed is a model with linear elasticity and isotropic hardening. Furthermore, the report contains comments and explanations to why the model proposed by Stenberg (2003) for the out-of-plane behaviour is not appropriate.

The implementation of the theoretical model requires a development of an integration scheme and, since ABAQUS/Standard uses an implicit approach, a material stiffness matrix consistent with the integration scheme. This has been done and the Newton-Raphson methods used have achieved quadratic convergence, which makes the model fast and easy to work with.

The simulations of creasing is done with the proposed continuum model together with the interface model proposed by Xia (2002). The simulations shows an improvement compared to the original model proposed by Xia (2002), mainly during unloading.

Contents

Acknowledgements **i**

Abstract **iii**

1 Introduction **1**
1.1 Background 1
1.2 Purpose of the assignment 2
1.3 Notation 2

2 Literature and experimental study **5**
2.1 A short introduction to paper and paperboard 5
2.2 Experimental background 8
2.2.1 In-plane behaviour 8
2.2.2 Out-of-plane behaviour 9
2.3 Short review of the 3DM model presented by Xia (2002) 10
2.3.1 Theory of the continuum model 12
2.3.2 Theory of the interface model 16

3 Theory of continuum model in a small deformation formalism **23**
3.1 Elastic strain of ortotropic materials and division into in-plane model and out-of-plane model. 23
3.2 In-plane model 26
3.2.1 Yield criterion 26
3.2.2 Flow rule 27
3.2.3 Hardening 30
3.3 Out-of-plane model 30
3.3.1 ZD compression 31
3.3.2 Out-of-plane shear 34

4 Implementation **37**
4.1 Solution of equilibrium equation 38
4.2 Integration of constitutive equations 40
4.3 Material tangent stiffness matrix 43

4.4 ABAQUS/Standard 44

5 Simulations and results **47**
5.1 Set-up in the simulations 47
5.2 Results 50

6 Discussion and conclusions **57**
6.1 Further work 58

A Comments to the model proposed by Stenberg (2003) **65**
A.1 ZD compression 65
A.2 Shear model 66

B Calculations used in the implementation **69**
B.1 In-plane model 69
B.1.1 Material tangent stiffness components 71
B.2 Out-of-plane normal model 71
B.2.1 Material tangent stiffness components 72
B.3 Out-of-plane shear model 72
B.3.1 Material tangent stiffness components 73

Chapter 1

Introduction

1.1 Background

Paper is a widely used material with many advantages; it is cheap to manufacture, it is fairly strong considering the low weight, it can be recycled and it does not contain large amounts of hazardous substances. It is a advantage to decrease the amount of raw material in the paper products both from an economic point of view and an environmental point of view. Solid mechanics analyses has been used in various areas to optimize products, and there exists many different material models for all kinds of material. This type of analyses can also be used in order to optimize paper and paperboard products, but in order to do this an accurate model for the material is needed. Solid mechanics analyses has only recently been introduced for calculation on paper and paperboard. The main reason for this is that paper and paperboard is a complex material to model; mainly because it has large differences in properties between the different directions and the fibres delaminate when the paperboard deforms. The four main reasons for creating a material model in order to do simulations on paper and paperboard are:

- Accurate predict outcome of converting processes.
- Establish important material properties, to get an idea of how the material will act when improvements of paper properties are achieved.
- Gather knowledge from experiments, to get an easy handled description of the paper.
- Understand the mechanisms of paper deformation.

STFI-Packforsk, which is the Swedish Pulp, Paper, Printing and Packaging Research Institute located in Stockholm, Sweden, has together with contributing paper industry recognized the need to develop a material model for paper and paperboard. Therefore they have for many years been involved in a large project that has involved experimental, theoretical and numerical studies. The model developed, called the 3DM-model, is based on a large

deformation formalism, and was published as PhD thesis by Q.S. Xia at Massachusetts Institute of Technology in the USA in 2002. The 3DM model consists of a continuum in-plane model that controls the behaviour in a layer of fibres in the paperboard and an interface model that controls the delaminations between the layers of fibres.

1.2 Purpose of the assignment

The objective of this master's thesis is to develop and implement a three dimensional continuum material model for layers of paper fibres based on small deformations. The model should together with an existing delamination model capture the behaviour of paperboard. The model should also be tested to verify the accuracy of the model. This is done by:

- Adapting the continuum model presented by Xia (2002) into a model based on small deformations.
- Improving the model presented by Xia (2002) by adding plastic behaviour in the through-thickness direction of the paper.
- Choosing an appropriate implementation strategy.
- Implementing the model into the finite element program ABAQUS/Standard.
- Testing the model by building up a creasing procedure in ABAQUS and do simulations on the paperboard.

1.3 Notation

Two types of notation are used in the report. Bold symbols refer to variables that consist of more than one component and are used in general discussions when specific components are of minor importance. When we need to be more specific and refer to each component index notation is used. Index notation is a convenient way of writing complex formulas in a compact form. Each index takes the values 1, 2 and 3 if nothing else is stated. If two indices are repeated in a term summation are applied, i.e.

$$A_{ij} \Leftrightarrow \begin{bmatrix} A_{11} & A_{12} & A_{13} \\ A_{21} & A_{22} & A_{23} \\ A_{31} & A_{32} & A_{33} \end{bmatrix}, \tag{1.1}$$

$$A_{ii} = \sum_{i=1}^{3} A_{ii} = A_{11} + A_{22} + A_{33}. \tag{1.2}$$

To illustrate the difference between index notation, to write out each component and bold notation see example below.

$$A_{ij}X_j = B_i \Leftrightarrow \begin{bmatrix} A_{11} & A_{12} & A_{13} \\ A_{21} & A_{22} & A_{23} \\ A_{31} & A_{32} & A_{33} \end{bmatrix} \begin{bmatrix} X_1 \\ X_2 \\ X_3 \end{bmatrix} = \begin{bmatrix} B_1 \\ B_2 \\ B_3 \end{bmatrix} \Rightarrow \boldsymbol{AX} = \boldsymbol{B} \tag{1.3}$$

In the report the Euclidean norm is used, defined as

$$\|\boldsymbol{x}\| = \sqrt{x_1^2 + ... + x_n^2} \quad \text{if} \quad \boldsymbol{x} = (x_1, ..., x_n). \tag{1.4}$$

Chapter 2

Literature and experimental study

2.1 A short introduction to paper and paperboard

The main constituents when manufacturing paper and paperboard are fibre, water and energy. Fibres from wood are by far the most common but fibres from grass and other plants - and in rare occasions fibres from outside the flora - can be used. In Sweden all paper mills uses wood as raw material. Wood contains fibres that hold together with lignin. When manufacturing paper the fibres need to be separated from each other. The two main methods to separate the fibres are the mechanical method and the chemical method. In the mechanical method the fibres are torn apart by adding mechanical energy with for example a grinding wheel. In the chemical method the fibres are separated by adding chemicals which resolve the lignin. With the mechanical method, the wood is better preserved since less of the lignin is removed. This also has the effect that paper made from fibres separated with the mechanical method is weaker and turn yellow faster than paper made from chemical pulp. The methods can be combined and heat and water can be added in the fibre separation to achieve different advantages and different properties in the paper. This is a big research area and numerous books have been written on the subject cf. Fellers and Norman (1998).

During or after the fibre separation process the fibres are resolved in water and this fibre suspension is sprayed onto a fast moving web, called a wire. In a pressing segment and a drying segment the water is drained out of the suspension and the fibres stick together with hydrogen bridges, hence no adhesives needs to be added.

The manufacturing process has the effect that most of the fibres are oriented in the direction of the machine and that almost no fibres are oriented in the thickness direction. This phenomenon leads to the anisotropy of paper. The paper is usually treated as an orthotropic material and the three different directions of the paper machine are used as principal directions of the paper. The directions are illustrated in figure 2.1. The paper

is highly anisotropic with the stiffness in the Machine Direction (MD) being 1-5 times larger than in the Cross Direction (CD), and around 100 times larger than in the thickness direction (ZD).

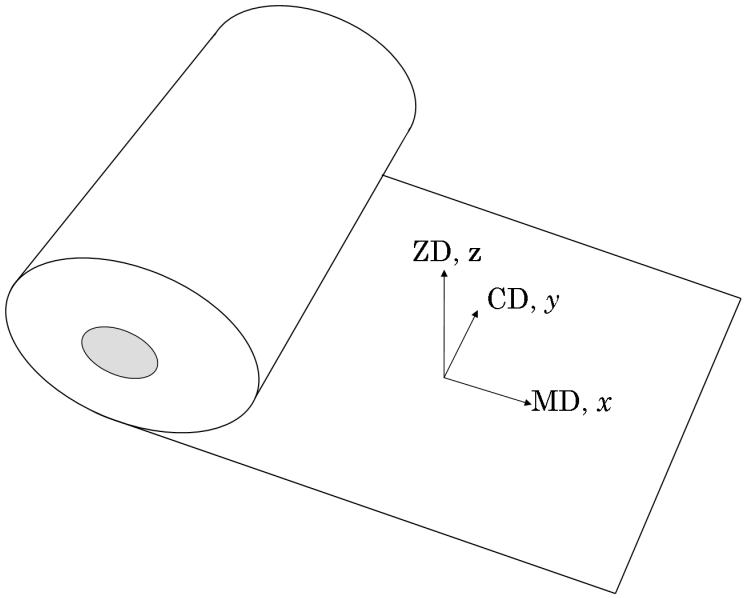

Figure 2.1: Principal directions in paper.

Paper materials exhibit many exciting features making them complex to model. This is due to their highly anisotropic behaviour, non-linear inelastic material response and dependency on the moisture content of the material. Furthermore, inelastic delamination between fibres occur when the paperboard deforms plastically, which makes a continuum approach not valid for the entire paperboard when modelling detailed inelastic behaviour where delamination occur.

Thicker paper materials is usually called paperboard, but there exists no distinct definition separating paper from paperboard. As a reference material in this work a multilayered paperboard has been used. The paperboard is composed of five layers; three layers made by mechanical pulp in the middle of the paperboard, and one outer chemical layer on each side of the core, see figure 2.2. The paperboard is approximately 0.45 millimetres thick.

When converting paperboard into products such as packages the paperboard needs to be folded. An illustration of this procedure can be seen in figure 2.3. To get a nice fold the paperboard is first punched with a male die (cf. figure 2.3.b), creating a straight line of damage in the paperboard. When a bending moment is applied to the paperboard (cf. figure 2.3.d) the fold will preferentially fold along this line creating a straight and symmetric crease.

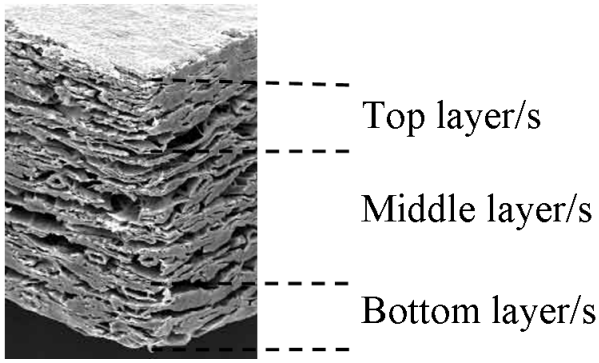

Figure 2.2: Picture of paperboard showing the different layers.

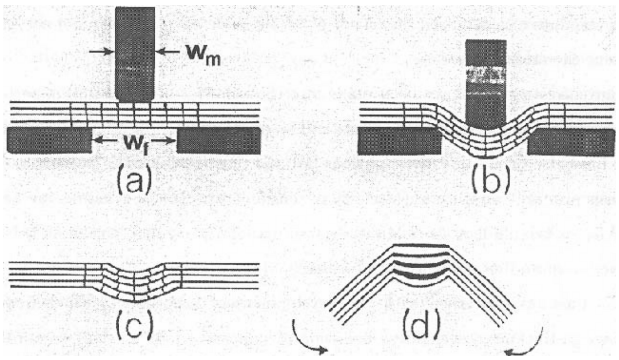

Figure 2.3: Schematic of creasing and subsequent folding of paperboard. From Carlsson et al. (1983).

2.2 Experimental background

In order to understand the elastic and inelastic mechanisms of paper and paperboard several experimental studies have been performed. To mention a few Stenberg (2002a) has studied the behaviour in the out-of-plane direction, deRuvo et al. (1980) has studied the in-plane biaxial failure surface and Dunn (2000) has studied the micro-mechanical behaviour in a Scanning Electron Microscope.

2.2.1 In-plane behaviour

The in-plane tensile behaviour for paperboard is presented in figure 2.4. These stress-strain curves plotted for MD, CD and an orientation 45° from MD clearly shows the anisotropic behaviour of paperboard. The curves depict that MD has a factor 2-3 higher elastic modulus and initial yield than CD. Tensile loading-unloading-reloading tests (Persson, 1991)

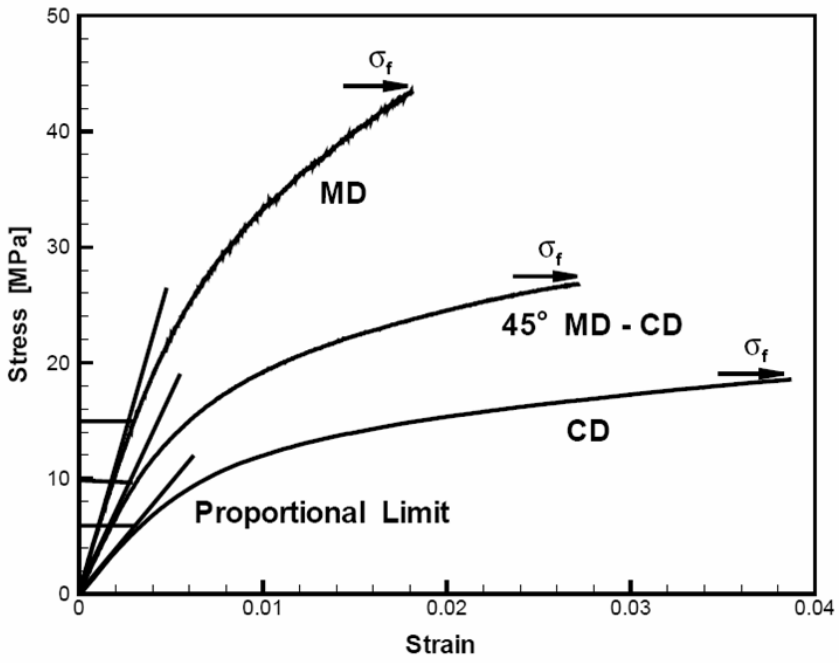

Figure 2.4: In-plane stress-strain curves, σ_f indicating failure stress. Adopted from Xia (2002).

show that the elastic tensile modulus is nearly unaffected by plastic strain, consistent with the traditional elasto-plasticity theory.

To determine the yield surface of paper data from multi-axial tests is required. However, tests for the initial yield surface and the evolvement with the plastic strain has not been examined. Several researchers have however obtained biaxial failure surfaces; deRuvo et al.

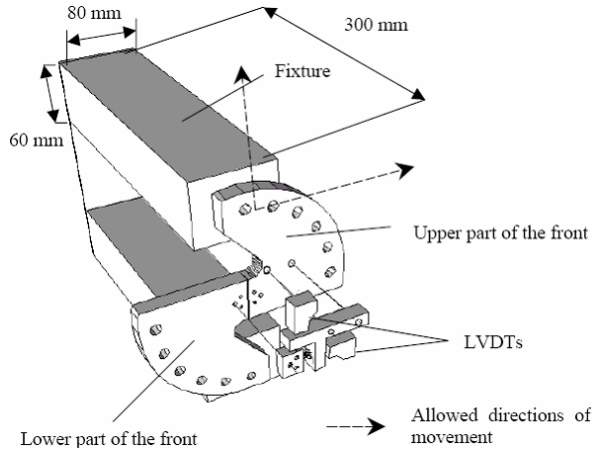

(a) The modified Arcan device for measuring the out-of-plane behaviour of paperboard. The test sample is glued between the two parts of the front. LVDT stands for Linear Variable Displacement Transducers and measures the displacements between the two parts of the front.

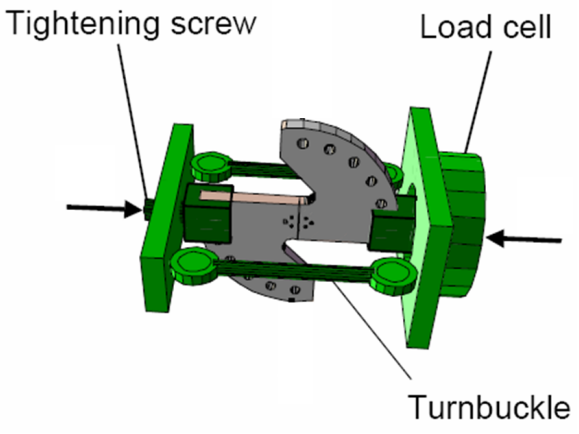

(b) Arcan device for compression tests.

Figure 2.5: The modified Arcan device. From Stenberg (2002b).

(1980), Fellers et al. (1981) and Gunderson (1983). Since the experimental data for the yield surface is unavailable it is usually assumed that the yield surface exhibits the same characteristic as the failure surface.

2.2.2 Out-of-plane behaviour

The out-of-plane stress-strain behaviour of paperboard has been studied using a modified Arcan (Arcan et al., 1978) device designed by Stenberg et al. (2001a). Figure 2.5(a) shows the schematic of the design and figure 2.5(b) shows the set up for compression. The samples measured 40 mm×15 mm for both compression and tension. A representative ZD tensile stress-strain curve for the paperboard obtained by Stenberg et al. (2001a) is shown in figure 2.6(b) The figure shows the peakload and subsequent softening. The stress-strain behaviour in ZD compression has been studied by Stenberg (2002b) and a typical curve for this behaviour is shown in figure 2.6(a). The curve shows the nonlinear elastic response and that the elastic response depends on the plastic deformation of the paperboard.

When paperboard is creased, in order to soften the structure, initial cracks develop that causes the paperboard to more easily delaminate in the subsequent folding. The micromechanical mechanisms in paperboard, including delamination, has been studied by Dunn (2000). Figure 2.7 shows the delamination of paperboard in ZD tension. The initial delamination of paperboard in a creasing procedure is shown in figure 2.8. Up until the delamination of the paperboard starts it can be a reasonable assumption to consider the

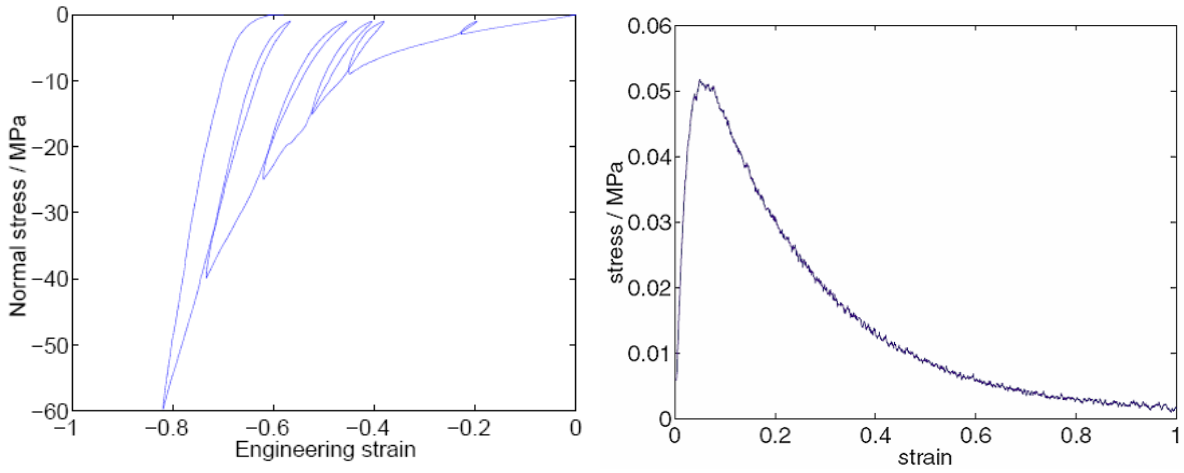

(a) A typical stress-strain curve for paperboard in compression, under consecutive through-thickness loadings and unloadings. Adopted from Stenberg et al. (2002b).

(b) A typical stress-strain curve for the paperboard in ZD tension. Adopted from Stenberg (2001a).

Figure 2.6: Stress-strain response of paperboard in ZD.

paper as a homogeneous material as long as the considered length scale is reasonably large. When the cracks initiate the homogeneous assumption is however not valid.

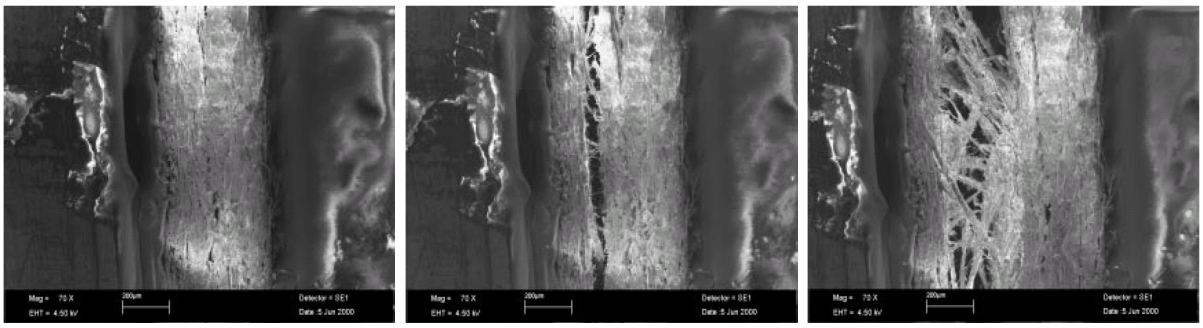

(a) (b) (c)

Figure 2.7: ZD tension test of paperboard. View of the MD plane. Pictures taken with Scanning Electron Microscope (SEM) by Dunn (2000).

2.3 Short review of the 3DM model presented by Xia (2002)

Through the years different approaches have been applied to describe the properties of paperboard. The models fall into mainly three different categories; network models, lam-

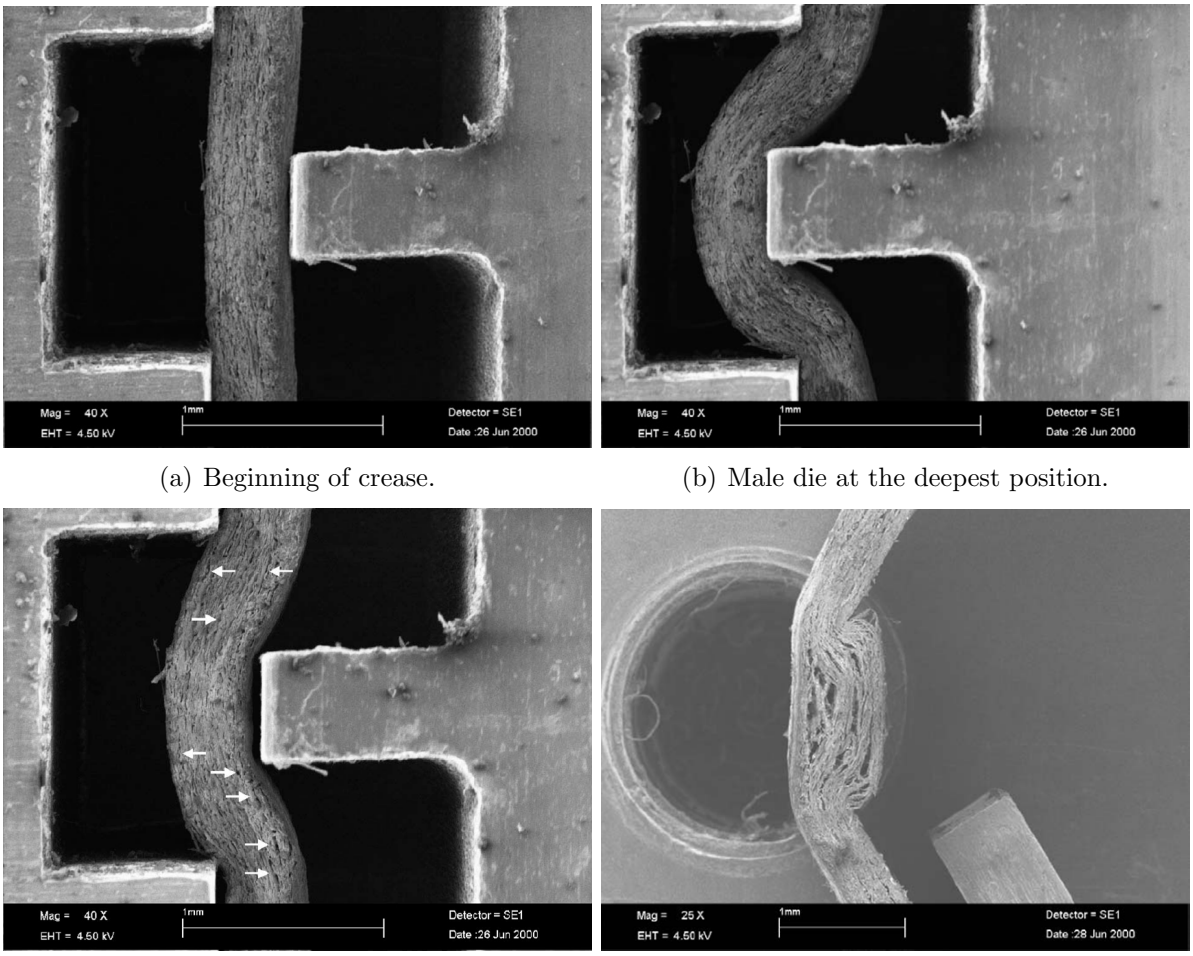

(a) Beginning of crease.

(b) Male die at the deepest position.

(c) End of crease. White arrows indicating initial delamination.

(d) Subsequent folding.

Figure 2.8: Crease and subsequent fold of paperboard across MD. Pictures taken with SEM by Dunn (2000).

inate models and continuum models. The models have advantages and disadvantages but none of them completely captures the behaviour of paperboard. The approach used by Xia (2002) is to use a continuum model together with an interface model. A schematic model of paperboard as presented by Xia (2002) can be seen in figure 2.9. The continuum model can in a sense be seen as the constitutive model for the mat of fibres in a plane, while the interface model accounts for the delamination between the mats of fibres.

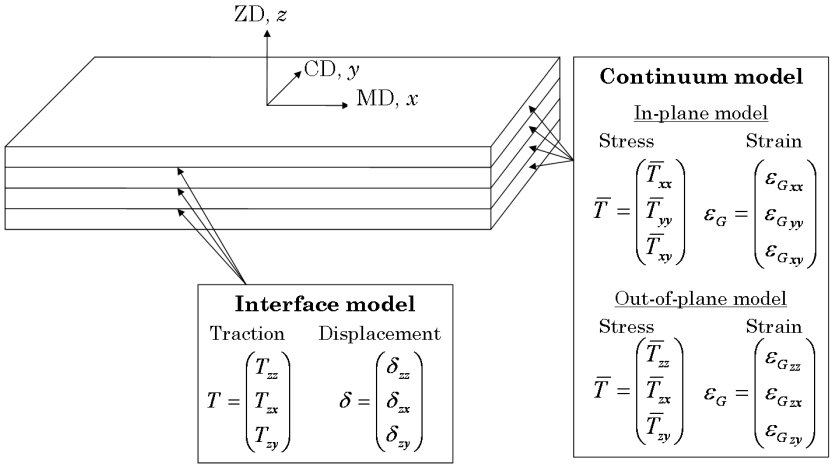

Figure 2.9: Schematics of Paperboard.

2.3.1 Theory of the continuum model

The continuum model proposed by Xia (2002) is controlling the behaviour of the mat of fibres. The model consist of the three components for the normal stress and strain in the three directions; and the the three components for the shear between these directions. In the model presented by Xia (2002) the components for compression and tension in MD and CD and the shear between the two have an elasto-plastic behaviour. This is henceforth referred to as the in-plane model. The compression and tension in ZD and the shear between ZD and the two in-plane directions has in the 3DM-model an elastic behaviour. The model for these three components is henceforth referred to as the out-of-plane model.

The elastic behaviour in the in-plane model is linear and orthotropic. The yield surface evolves with the plastic strain with an isotropic hardening, meaning that the yield surface does only depend on the magnitude of the plastic strain and not on the direction. The plastic flow is modelled with an associate flow rule[1]. The model is formulated in a large

[1]Strictly, the flow rule is not associate since the flow rule is not energy conjugate as reported by Ristinmaa (2003)

deformation formalism. In this section the theory of the model is outlined. For more details about the theory and how the model should be calibrated cf. Ristinmaa (2003).

Stress-strain relationship

The displacement of a particle can be described by considering the particle's reference position in a coordinate system, $\boldsymbol{X}$, and its current position, $\boldsymbol{x}$ according to figure 2.10. The displacement, $\boldsymbol{u}$, is then defined as

$$\boldsymbol{u} = \boldsymbol{x} - \boldsymbol{X}. \tag{2.1}$$

Two neighbouring particles at a reference configuration in a continuous body can be

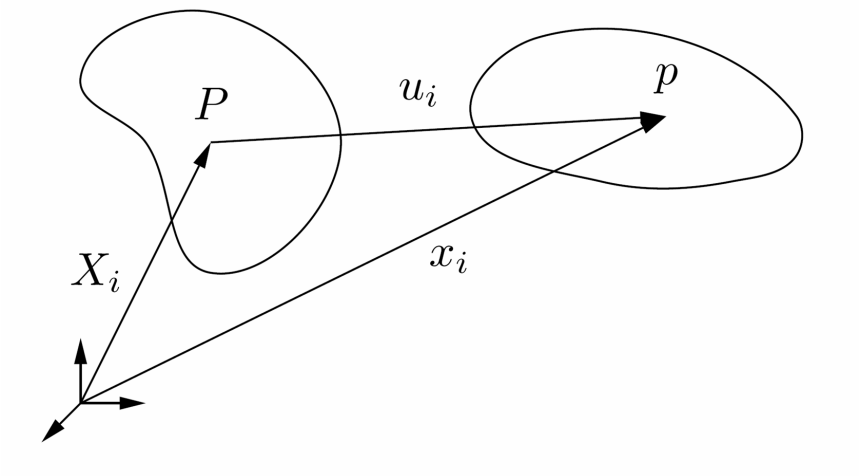

Figure 2.10: Displacement u_i from the reference configuration, X_i, to the current configuration, x_i.

identified by their positions $\boldsymbol{X}$ and $\boldsymbol{X} + d\boldsymbol{X}$ where $\boldsymbol{X}$ denotes a position vector and $d\boldsymbol{X}$ the distance between the particles. After deformation of the body the new distance between the particles is $d\boldsymbol{x}$. It is possible to describe the change from the reference configuration to the current configuration without including the rigid body motion according to

$$d\boldsymbol{x} = \frac{\partial \boldsymbol{x}}{\partial \boldsymbol{X}} d\boldsymbol{X} = \boldsymbol{F} d\boldsymbol{X}, \tag{2.2}$$

where $\boldsymbol{F}$ is the linear mapping known as the deformation gradient, cf. figure 2.11. To make the mapping unique it is assumed that $det(\boldsymbol{F}) > 0$.

With equation (2.1) and equation (2.2) it is seen that the deformation gradient can also be written as

$$\boldsymbol{F} = \frac{\partial \boldsymbol{x}}{\partial \boldsymbol{X}} = \frac{\partial}{\partial \boldsymbol{X}}(\boldsymbol{X} + u) = \boldsymbol{I} + \frac{\partial \boldsymbol{u}}{\partial \boldsymbol{X}}. \tag{2.3}$$

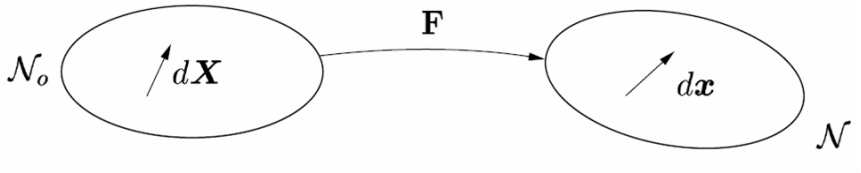

Figure 2.11: Deformation of a continuous body.

It is assumed that at each material point the total deformation gradient can be multiplicatively decomposed into an elastic part, $\boldsymbol{F}^e$, and a plastic part, $\boldsymbol{F}^p$, (cf. figure 2.12) hence

$$\boldsymbol{F} = \boldsymbol{F}^e \boldsymbol{F}^p. \tag{2.4}$$

When large deformations are considered many different strain measures exist. The optimal

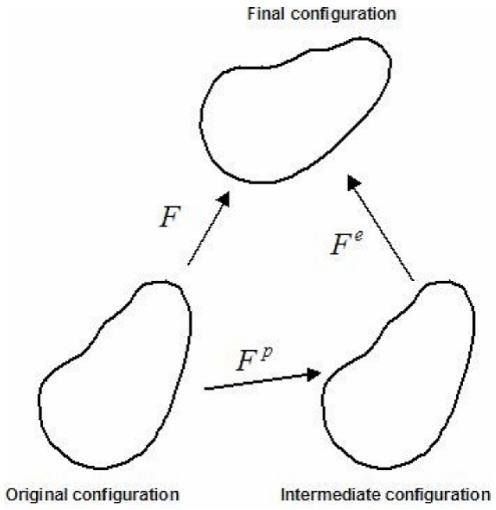

Figure 2.12: Schematic representation of the multiplicative decomposition into elastic and plastic parts.

choice of strain depends on the material behaviour and type of analysis and there is no true strain as there is a true stress. The model uses the Green strain[2], $\boldsymbol{\varepsilon}_G$, defined as

$$\boldsymbol{\varepsilon}_G \equiv \frac{1}{2}(\boldsymbol{F}^T\boldsymbol{F} - \boldsymbol{I}) = \frac{1}{2}\left(\frac{\partial u_i}{\partial X_j} + \frac{\partial u_j}{\partial X_i} + \frac{\partial u_k}{\partial X_i}\frac{\partial u_k}{\partial X_j}\right). \tag{2.5}$$

According to Xia (2002) the second Piola-Kirchoff stress in the intermediate configuration, $\bar{\mathbf{T}}$, is related to the elastic Green strain, $\boldsymbol{\varepsilon}_G^e$ using the linear relationship

$$\bar{\boldsymbol{T}} = \boldsymbol{C}\boldsymbol{\varepsilon}_G^e, \tag{2.6}$$

[2]This strain measure is computationally convenient for problems involving large motions but small strains, since it can be computed directly from the deformation gradient.(ABAQUS, 2004)

where $\boldsymbol{C}$ is the fourth order elasticity tensor which is taken to be orthotropic. Both $\bar{\boldsymbol{T}}$ and $\boldsymbol{\varepsilon}_G^e$ are related to an intermediate configuration, which is the deformed configuration from which the elastic deformation has been removed. We will go into more details about the elasticity tensor in connection with small strains in the next chapter. The evaluation of plastic strains are governed by

$$\dot{\boldsymbol{F}}^p = \boldsymbol{l}^p \boldsymbol{F}^p, \tag{2.7}$$

where $\boldsymbol{l}^p$ is the plastic velocity gradient.

In the model proposed by Xia (2002) plastic deformation in out-of-plane compression is not considered. Instead, an elastic through-thickness relationship is used under ZD compression and shear. The through-thickness elastic moduli, E_z, G_{zx} and G_{zy} are taken to be exponential functions of the ZD strain under compression as follows

$$\begin{aligned} E_z &= E_z^0 e^{-a\varepsilon^e_{G,zz}} \quad (when\ \varepsilon^e_G < 0), \\ G_{zx} &= G_{zx}^0 e^{-b\varepsilon^e_{G,zz}} \quad (when\ \varepsilon^e_G < 0), \\ G_{zy} &= G_{zy}^0 e^{-c\varepsilon^e_{G,zz}} \quad (when\ \varepsilon^e_G < 0), \end{aligned} \tag{2.8}$$

where $\varepsilon^e_{G,zz}$ is the ZD elastic strain component and a,b and c are material constants determined from fitting of the compressive through-thickness stress-strain curves. For ZD tension we simply have $E_z = E_z^0$, $G_{zx} = G_{zx}^0$ and $G_{zy} = G_{zy}^0$. Note that the nonlinear shear elasticity given by the two last equations in (2.8) was not included in Xia (2002) but was included in the implementation done by Xia, and is now considered as a part of the 3DM model, cf. Nygårds (2005).

Yield criterion and hardening

Since it is assumed that the model only exhibits plastic behaviour in the in-plane directions the out-of-plane stress components are not considered in the yield criteria. Thus, stress components $\bar{T}_{xx}$, $\bar{T}_{yy}$ and $\bar{T}_{xy}$ are the only ones used in the yield and flow equations.

A new yield criterion was proposed by Xia (2002) since no existing criteria successfully described the experimental data available in the literature. Other criteria that are commonly used to fit in the failure surface of paper is the criterion originally proposed by Hill (1950) and the one proposed by Tsai and Wu (1971). Xia (2002) assumes that the yield surface can be constructed by n sub-surfaces, where $\boldsymbol{N}_I$ is the normal to the Ith subsurface. The yield criterion is expressed as

$$f(\bar{\boldsymbol{T}}, \bar{\gamma}) = \sum_{I=1}^{n} \chi_I \left(\frac{\bar{\boldsymbol{T}} : \boldsymbol{N}_I}{S_I(\bar{\gamma})} \right)^{2k} - 1 \tag{2.9}$$

where $2k$ is a material constant with the value being a positive integer, $S_I(\bar{\gamma})$ are the equivalent strengths corresponding to the sub-surfaces i.e. this function includes the hardening

of the model, $\bar{\gamma}$ is the equivalent plastic strain defined as $\bar{\gamma} = \int \dot{\bar{\gamma}} dt$ and χ_I is a switching control with the properties

$$\chi_I = \begin{cases} 1 & \text{if } \bar{\boldsymbol{T}} : \boldsymbol{N}_I > 0; \\ 0 & \text{otherwise.} \end{cases} \tag{2.10}$$

Xia (2002) assumes that the yield strength evolution can be fitted to

$$\begin{aligned} S^I(\bar{\gamma}) &= S_0^I + A_1 tanh(B_1\bar{\gamma}) + C_1\bar{\gamma}, & (2.11)\\ S^{II}(\bar{\gamma}) &= S_0^{II} + A_2 tanh(B_2\bar{\gamma}) + C_2\bar{\gamma}, & (2.12)\\ S^{III}(\bar{\gamma}) &= S_0^{III} + A_3 tanh(B_3\bar{\gamma}) + C_3\bar{\gamma}, & (2.13)\\ S^{IV}(\bar{\gamma}) &= S_0^{IV} + A_4 tanh(B_4\bar{\gamma}) + C_4\bar{\gamma}, & (2.14)\\ S^{V}(\bar{\gamma}) &= S_0^{V} + A_5 tanh(B_5\bar{\gamma}) + C_5\bar{\gamma}, & (2.15)\\ S^{VI}(\bar{\gamma}) &= S^{III}(\bar{\gamma}). & (2.16) \end{aligned}$$

In connection with small deformations in the next chapter the yield surface will be more extensively described.

Evolution laws

The plastic flow is defined as

$$\boldsymbol{l}^p = \bar{\gamma}\boldsymbol{K}, \tag{2.17}$$

where $\boldsymbol{l}^p$ is the plastic velocity gradient. $\bar{\gamma}$ is the magnitude of plastic stretching rate, and $\boldsymbol{K}$ is the normalized flow direction and is calculated as

$$\boldsymbol{K} = \frac{\hat{\boldsymbol{K}}}{||\hat{\boldsymbol{K}}||}, \tag{2.18}$$

where $\hat{\boldsymbol{K}}$ is the derivative of the yield surface and is assumed to be

$$\hat{\boldsymbol{K}} = \frac{\partial f}{\partial \bar{\boldsymbol{T}}}. \tag{2.19}$$

With the aid of the yield surface, the yield direction can be calculated as

$$\hat{\boldsymbol{K}} = \frac{\partial f}{\partial \bar{\boldsymbol{T}}} = 2k \sum_{I=1}^{n} \left(\frac{\bar{\boldsymbol{T}} : \boldsymbol{N}_I}{S^I(\bar{\gamma})} \right)^{2k-1} \chi_I \frac{\boldsymbol{N}_I}{S^I(\bar{\gamma})}. \tag{2.20}$$

2.3.2 Theory of the interface model

It is outside the scope of this report to go into details in the interface model. However, the model is used in the simulations of creasing and folding of paperboard. Therefore, a summary of the theoretical framework behind the model is presented.

The model is important since two major mechanisms dominate during deformation of paperboard, namely elasto-plastic deformation within plies and delamination between plies. Just one continuum model can not capture the plastic behaviour in paperboard in shear. To illustrate this let us consider a two dimensional model of paper in the ZD-MD direction modelled with a continuum model, cf. figure 2.13. In a model like this the three components

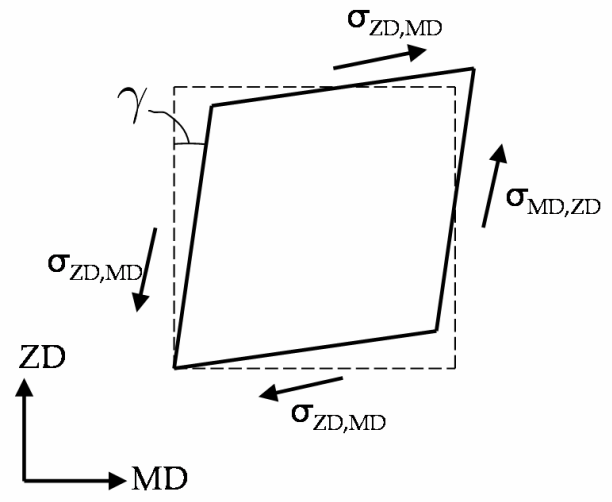

Figure 2.13: A continuum element subjected to shear.

of importance are ZD, MD and the shear between MD and ZD. In a continuum model the MD-ZD shear is not different from the ZD-MD shear[3]. We know that the plies slip easier in the direction of the fibres. Hence a unit of shear strain along the fibres, $\varepsilon_{ZD,MD}$, causes lower shear stress along the fibre, $\sigma_{ZD,MD}$, than a unit of shear strain across the fibres, $\varepsilon_{MD,ZD}$, causes the stress across the fibres, $\sigma_{MD,ZD}$. However, this is as mentioned earlier impossible with only one continuum model.

The delamination model in this work has been proposed by Xia (2002). The model is traction-displacement based and models an elasto-plastic cohesive law between two opposing surfaces. The model is used between the layers of in-plane elements (layers of fibres in real life paper[4]) and takes care of the delamination between the fibres. To simplify the understanding of the theory consider an interface between two plies in a paperboard as depicted in Figure 2.14. At each point of the interface we introduce a local coordinate system where n is normal to the interface and t_1 and t_2 are orthogonal tangents to the interface. The t_1- and t_2-directions usually corresponds to the MD and CD directions of paperboard, respectively. For brevity in the equation expressions, let 1, 2 and 3 denote n, t_1 and t_2.

[3]This is the reason why engineering shear strains can be used which are defined $\gamma_{xy} = \varepsilon_{xy} + \varepsilon_{yx} = 2\varepsilon_{xy}$. As curiosity it can be mentioned that in gradient theory polarities can occur that makes $\sigma_{xy} \neq \sigma_{yx}$

[4]Although in simulations an approximation is introduced, since the layers where the interface model is introduced and the model is allowed to delaminate, is usually fewer than the delamination areas in the paperboard.

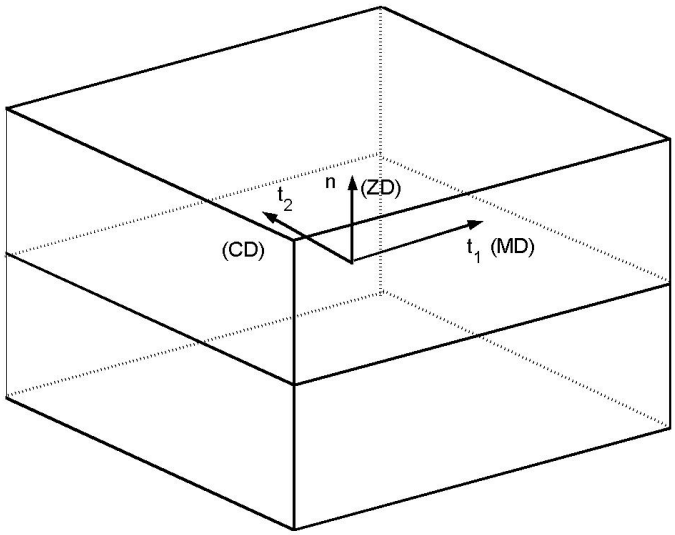

Figure 2.14: An interface between two paperboard plies.

Indices indicated by Greek letters imply that no summation should be carried out over repeated indices. Whenever other indices are used summation according to the summation convention explained in section 1.3 should be used, i.e.

$$a_\alpha b_\alpha = a_\alpha b_\alpha \quad \text{(no summation)}, \tag{2.21}$$

$$a_i b_i = \sum_{i=1}^{n} a_i b_i. \tag{2.22}$$

Kinematics

It is assumed that the displacement between two opposing surfaces can be divided into an elastic part and a plastic part. Thus, with reference to a local coordinate system at the interface each displacement component can be expressed as

$$\delta_i = \delta_i^e + \delta_i^p. \tag{2.23}$$

Constitutive equations

According to Xia (2002) a change in traction across the interface due to an incremental change of displacements is expressed as

$$\Delta T_\alpha = K_\alpha \left(\Delta\delta_\alpha - \Delta\delta_\alpha^p \right), \tag{2.24}$$

where K_α denotes the components of the instantaneous interface stiffness in the α-direction. The instantaneous interface stiffness will decrease as the interface deforms. It depends on the equivalent plastic displacement ($\bar{\delta}^p$) according to

$$K_\alpha(\bar{\delta}^p) = K_\alpha^0 \left(1 - \chi R_\alpha^k D(\bar{\delta}^p)\right), \tag{2.25}$$

where K_α^0 is the initial interface stiffness and $D(\bar{\delta}^p)$ is the interface damage. It is a positive scalar that is derived as

$$D(\bar{\delta}^p) = tanh\left(\frac{\bar{\delta}^p}{\delta_0^p}\right) = tanh\left(\frac{\bar{\delta}^p}{C}\right). \tag{2.26}$$

Hence, the model accounts for a reduced stiffness of the interface as damage evolves in the interface. In equation (2.25) R_α^k and C are material constants, and the incremental equivalent plastic displacement in Eq. (2.26) is expressed as

$$\Delta\bar{\delta}^p = \|\Delta\delta_i^p\|. \tag{2.27}$$

The interface is formulated to account for delamination in tension and shear. It is not at all desired to have overlapping of the surfaces when loaded in ZD compression. Therefore, penalty functions are used to prevent overlapping under such circumstances.

Yield criterion

Since the delamination model is elasto-plastic a yield condition is introduced. The yield condition is equivalent with a yield surface, but is expressed in terms of tractions. The proposed yield conditions rely on experimental data by Stenberg (2002a), and Xia (2002) expressed that yielding occurs when

$$f(T, \bar{\delta}^p) = \sum_{\alpha=2}^{n} \frac{S_1 T_\alpha^2}{S_\alpha(\bar{\delta}^p)^2} + T_1 - S_1 = 0, \tag{2.28}$$

where $S_\alpha(\bar{\delta}^p)$ are the instantaneous interface strengths that depend on the equivalent plastic displacement, $\bar{\delta}^p$, according to

$$S_\alpha(\bar{\delta}^p) = S_\alpha^0 \left(1 - \chi R_\alpha^s D(\bar{\delta}^p)\right), \tag{2.29}$$

where S_α^0 are the initial interface strengths. In equation (2.28) n is used to distinguish between the 2-D case and 3-D case. In the 2-D case n equals 2, while in the 3-D case n is equal to 3. In figure 2.15 the two dimensional yield surface is plotted.

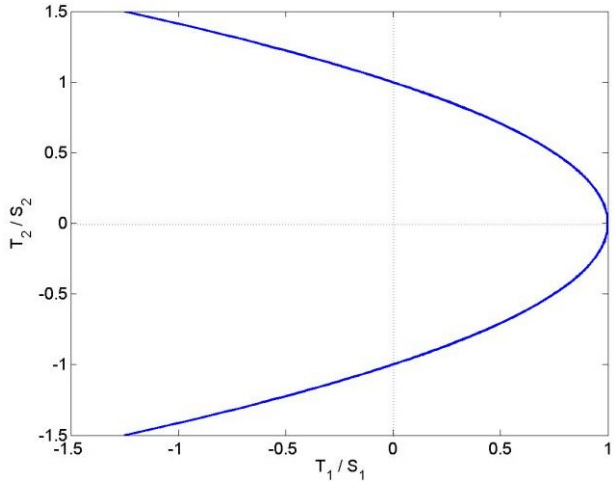

Figure 2.15: The yield surface in the case T_3=0.

Flow rule

According to Xia (2002) the plastic flow rule is written as

$$\Delta\delta_i^p = \chi\Delta\bar{\delta}^p M_i \tag{2.30}$$

where M_i are the components of the unit flow direction, i.e.

$$M_i = \frac{\hat{M}_i}{||\hat{\boldsymbol{M}}||} \tag{2.31}$$

and χ indicates if there is plastic deformation in the interface, it is defined as

$$\chi = \begin{cases} 1 & \text{if } f = 0 \text{ and } d\boldsymbol{T^*} \cdot \frac{\partial f}{\partial \boldsymbol{T}} > 0; \\ 0 & \text{if } f < 0 \text{ or } f = 0 \text{ and } d\boldsymbol{T^*} \cdot \frac{\partial f}{\partial \boldsymbol{T}} < 0. \end{cases} \tag{2.32}$$

For associated flow the components of the plastic flow direction is derived as

$$\hat{M}_1 = \frac{\partial f}{\partial T_1} = 1 \tag{2.33}$$

$$\hat{M}_\alpha = \frac{\partial f}{\partial T_\alpha} = 2\frac{S_1(\bar{\delta}^p)}{S_\alpha(\bar{\delta}^p)^2}T_\alpha. \quad \alpha = 2,3 \tag{2.34}$$

The associated flow will cause some normal dilation under the action of only shear stress, because of the shape of the traction yield surface. However, it is experimentally observed that the dilation in paperboard exceeds the dilation caused by associate flow. Therefore, a non-associate flow is used to capture the observed behaviour. For the non-associate flow the normal component of the flow direction is instead defined as

$$\hat{M}_1 = \mu(\bar{\delta}^p)\frac{\partial f}{\partial T_1}, \tag{2.35}$$

where μ is a frictional function, plotted in figure 2.16 defined as

$$\mu(\bar{\delta}^p) = A(1 - BD(\bar{\delta}^p)). \tag{2.36}$$

A and B are constants. $D(\bar{\delta}^p)$ is the parameter controlling the damage of the interface according to equation (2.26).[5]

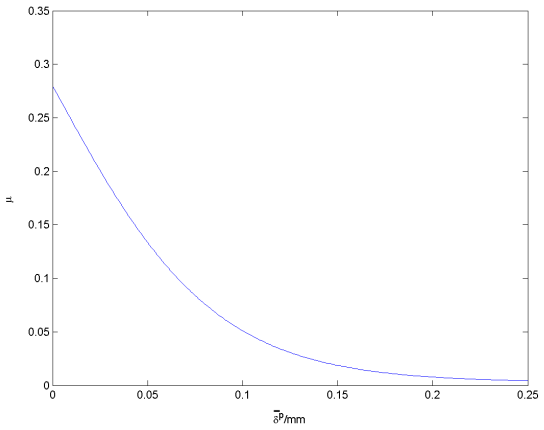

Figure 2.16: The frictional function plotted with parameters from Xia (2002).

[5]With the parameters for the frictional function fitted by Xia (2002) the non-associate flow rule proposed actually has lower normal dilation than for an associate flow rule as can be seen in figure 2.16, which contradicts the written purpose.

Chapter 3

Theory of continuum model in a small deformation formalism

In this chapter the theory of a continuum model based on small deformations is presented. In section 3.1 the Generalized Hooke's law is presented and the elastic response for paper is outlined. In section 3.2 a model for the in-plane components will be proposed that is a small deformation version of the model proposed by Xia (2002). In section 3.3 a model for the out-of-plane components will be proposed where the paperboard is treated as a foam-like material when compressed in the thickness direction.

3.1 Elastic strain of ortotropic materials and division into in-plane model and out-of-plane model.

We are interested in the response of paper and paperboard when loads and displacements are applied to the structure. For this we need to relate the kinematics of the structure to the stress in the structure. The strain is the link between the kinematics and the material model. If we recall the definition of the Green strain,

$$\boldsymbol{\varepsilon}_G \equiv \frac{1}{2}\left(\frac{\partial u_i}{\partial X_j} + \frac{\partial u_j}{\partial X_i} + \frac{\partial u_k}{\partial X_i}\frac{\partial u_k}{\partial X_j}\right), \tag{3.1}$$

where no assumptions were made. The strain in small deformations, $\boldsymbol{\varepsilon}$, relates the deformation of the body to the original configure and the assumptions of small strains cancel out the quadratic terms in equation (3.1) and we get

$$\varepsilon_{ij} = \frac{1}{2}\left(\frac{du_i}{dX_j} + \frac{du_j}{dX_i}\right). \tag{3.2}$$

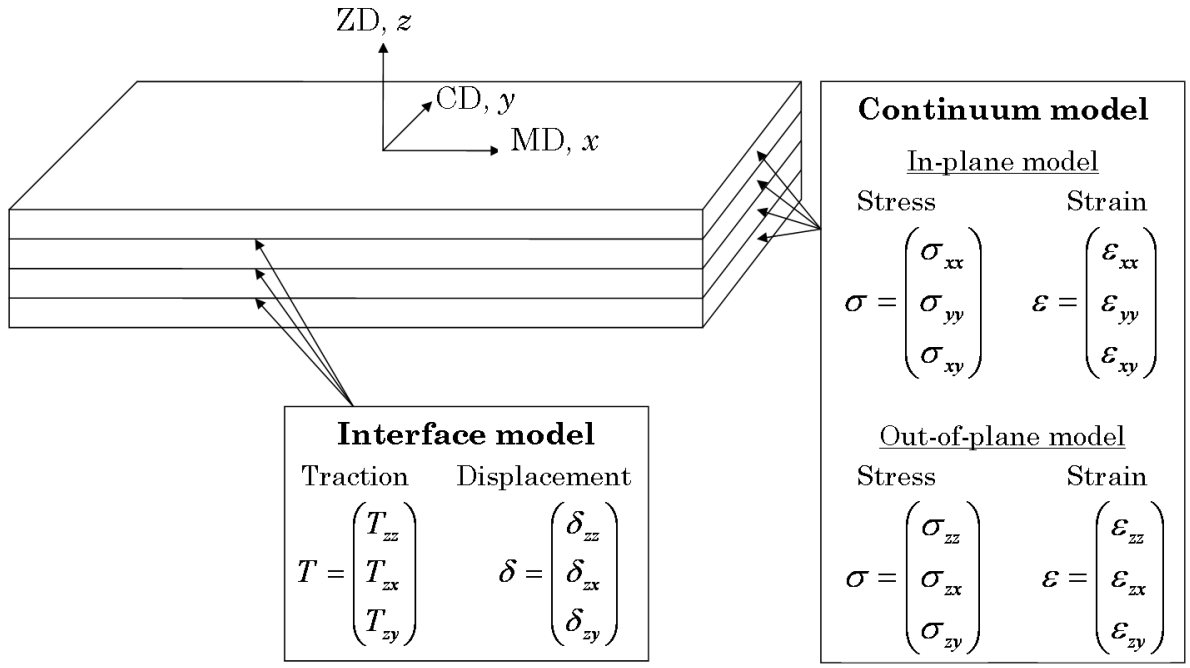

Figure 3.1: Schematics of Paperboard.

The total strain can be divided in an elastic part and a plastic part.

$$\varepsilon_{ij} = \varepsilon^e_{ij} + \varepsilon^p_{ij} \tag{3.3}$$

The relation that couples strain to stress, the constitutive model, describes the material. In 1676 Robert Hooke proposed a linear constitutive equation for the one dimensional case, $\sigma = E\epsilon^e$. This equation in its most general form is known as the Generalized Hooke's law,

$$\sigma_{ij} = D_{ijkl}\varepsilon^e_{kl}. \tag{3.4}$$

where σ_{ij} is the stress tensor which is defined as force acting on area of the original configuration. D_{ijkl} is the constant elastic stiffness tensor. Equation (3.4) and (3.3) gives

$$\sigma_{ij} = D_{ijkl}\left(\varepsilon_{kl} - \varepsilon^p_{kl}\right). \tag{3.5}$$

In static solid mechanics this equation forms a stable ground on which to build. The tensor D_{ijkl} introduced in equation (3.4) has 81 components but with energy considerations, geometrical considerations and considerations of the first law of thermodynamics it can be shown that a material can have no more than 21 independent components. Currently there is no useful engineering materials with 21 different and independent components (Lagace, 2005). Linear elastic orthotropic materials have 9 independent components, and equation

(3.4) can be written as

$$\begin{bmatrix} \sigma_{xx} \\ \sigma_{yy} \\ \sigma_{zz} \\ \sigma_{xy} \\ \sigma_{xz} \\ \sigma_{yz} \end{bmatrix} = \begin{bmatrix} \frac{1-\nu_{yz}\nu_{zy}}{E_y E_z \Delta} & \frac{\nu_{yx}+\nu_{zx}\nu_{yz}}{E_y E_z \Delta} & \frac{\nu_{zx}+\nu_{yx}\nu_{zy}}{E_y E_z \Delta} & 0 & 0 & 0 \\ \frac{\nu_{xy}+\nu_{xz}\nu_{zy}}{E_z E_x \Delta} & \frac{1-\nu_{zx}\nu_{xz}}{E_z E_x \Delta} & \frac{\nu_{zy}+\nu_{zx}\nu_{xy}}{E_z E_x \Delta} & 0 & 0 & 0 \\ \frac{\nu_{xz}+\nu_{xy}\nu_{yz}}{E_x E_y \Delta} & \frac{\nu_{yz}+\nu_{xz}\nu_{yx}}{E_x E_y \Delta} & \frac{1-\nu_{xy}\nu_{yx}}{E_x E_y \Delta} & 0 & 0 & 0 \\ 0 & 0 & 0 & G_{xy} & 0 & 0 \\ 0 & 0 & 0 & 0 & G_{xz} & 0 \\ 0 & 0 & 0 & 0 & 0 & G_{yz} \end{bmatrix} \begin{bmatrix} \varepsilon^e_{xx} \\ \varepsilon^e_{yy} \\ \varepsilon^e_{zz} \\ \gamma^e_{xy} \\ \gamma^e_{xz} \\ \gamma^e_{yz} \end{bmatrix} \tag{3.6}$$

with

$$\Delta = \frac{1 - \nu_{xy}\nu_{yx} - \nu_{yz}\nu_{zy} - \nu_{zx}\nu_{xz} - 2\nu_{xy}\nu_{yz}\nu_{zx}}{E_x E_y E_z}. \tag{3.7}$$

In equation (3.6) engineering shear strain is used and this will be used in the remainder of the report. Engineering shear strain is related to tensorial shear strain according to

$$\varepsilon = \begin{bmatrix} \varepsilon_{xx} \\ \varepsilon_{yy} \\ \varepsilon_{zz} \\ 2\varepsilon_{xy} \\ 2\varepsilon_{xz} \\ 2\varepsilon_{yz} \end{bmatrix} = \begin{bmatrix} \varepsilon_{xx} \\ \varepsilon_{yy} \\ \varepsilon_{zz} \\ \gamma_{xy} \\ \gamma_{xz} \\ \gamma_{yz} \end{bmatrix}. \tag{3.8}$$

From the definition of orthotropic materials equation (3.6) is symmetric. Hence the elastic Poisson's ratios and the elastic moduli are related according to

$$\frac{\nu_{xy}}{E_x} = \frac{\nu_{yx}}{E_y}, \tag{3.9}$$

$$\frac{\nu_{xz}}{E_x} = \frac{\nu_{zx}}{E_z}, \tag{3.10}$$

$$\frac{\nu_{yz}}{E_y} = \frac{\nu_{zy}}{E_z}, \tag{3.11}$$

where E_x, E_y and E_z are the Young's moduli in the principal directions. The Poisson's ratios, ν_{ij}, is defined as

$$\nu_{ij} = -\frac{\varepsilon_{jj}}{\varepsilon_{ii}} \quad \text{(no summations)}. \tag{3.12}$$

The out-of-plane Poisson's ratio in paper has been reported as both positive and negative (Öhrn, 1965; Baumgarten and Göttsching, 1973; Mann et al., 1980; Persson, 1991; Stenberg and Fellers, 2002), with the reports for most of the papers tested having a negative Poisson's ratio. The tests are however difficult to perform with many possible errors and when modelling paper the out-of-plane Poisson's ratios are often considered zero (Stenberg, 2003; Nygårds, 2005). Also in this model this assumption will be utilized, hence

$$\nu_{yx} = \nu_{xy} = \nu_{yz} = \nu_{zy} = 0. \tag{3.13}$$

Since the out-of-plane Poisson's ratios are zero and the out-of-plane properties are assumed not to depend on the in-plane state and vice versa. The in-plane and out-of-plane problem can be separated and solved independently. Thus, the in-plane problem is formulated as

$$\begin{bmatrix} \sigma_{xx} \\ \sigma_{yy} \\ \sigma_{xy} \end{bmatrix} = \begin{bmatrix} \frac{E_x}{1-\nu_{xy}\nu_{yx}} & \frac{\nu_{yx}E_x}{1-\nu_{xy}\nu_{yx}} & 0 \\ \frac{\nu_{xy}E_y}{1-\nu_{xy}\nu_{yx}} & \frac{E_y}{1-\nu_{xy}\nu_{yx}} & 0 \\ 0 & 0 & G_{xy} \end{bmatrix} \begin{bmatrix} \varepsilon_{xx} \\ \varepsilon_{yy} \\ \gamma_{xy} \end{bmatrix}. \tag{3.14}$$

The out-of-plane problem takes the form

$$\begin{bmatrix} \sigma_{zz} \\ \sigma_{xz} \\ \sigma_{yz} \end{bmatrix} = \begin{bmatrix} E_z & 0 & 0 \\ 0 & G_{xz} & 0 \\ 0 & 0 & G_{yz} \end{bmatrix} \begin{bmatrix} \varepsilon^e_{zz} \\ \gamma^e_{xz} \\ \gamma^e_{yz} \end{bmatrix}. \tag{3.15}$$

It should be noted that the linear relation in the through-thickness direction implied by equation (3.15) does not hold, as can be seen in figure 2.6(a). Instead a nonlinear expression is needed to capture the nonlinear out-of-plane elasticity of paperboard.

3.2 In-plane model

The in-plane model correlates the two in-plane normal strain components (ε_{xx} and ε_{yy}) and the in-plane shear strain component (γ_{xy}) to the corresponding stress components (σ_{xx}, σ_{yy} and σ_{xy}). The elastic response is governed by equation (3.14).

3.2.1 Yield criterion

The yield criterion tests if plasticity develops. The response is elastic inside the yield surface. In this work the yield criterion proposed by Xia (2002) is utilized, which in small deformations is formulated as

$$f(\boldsymbol{\sigma}, \varepsilon^p_{eff}) = \sum_{I=1}^{n} \chi_I \left(\frac{\boldsymbol{\sigma} : \mathbf{N}_I}{\sigma^I_s(\varepsilon^p_{eff})} \right)^{2k} - 1. \tag{3.16}$$

This yield surface is constructed by n yield planes. Xia (2002) uses six yield planes, one for every "direction" (i.e. σ_{xx} tension, σ_{xx} compression, σ_{yy} tension, σ_{yy} compression, positive τ_{xy} and negative τ_{xy}). Each yield plane is defined by the out pointing normal, $\boldsymbol{N}$, and the parameter controlling the size of the yield surface, σ_s. σ_s (σ_{s0} at the initial state) is defined, for the four planes for compression and tension, as the perpendicular distance from the origin to the plane yield planes, cf. figure 3.2. According to Xia (2002) this is also the definition for yield planes corresponding to shear, this is however *not* true. This distance for the shear planes is just $\frac{\sigma^{III}_s}{2N^{III}_{13}}$, or with the calibration procedure proposed by

Xia (2002) - and described in the next section - $\frac{\sigma_s^{III}}{\sqrt{2}}$ i.e. around 71% of σ_s^{III}. In conclusion, it is important to note that σ_{s0} (S_0 for large deformations) is *not* the yield stress in the different directions as it is sometimes mistaken for in the literature. The exponent $2k$ is governing the smoothening between the planes, a higher k results in a sharper edge, cf. figure 3.2. In equation (3.16) χ_I is a switch controller,

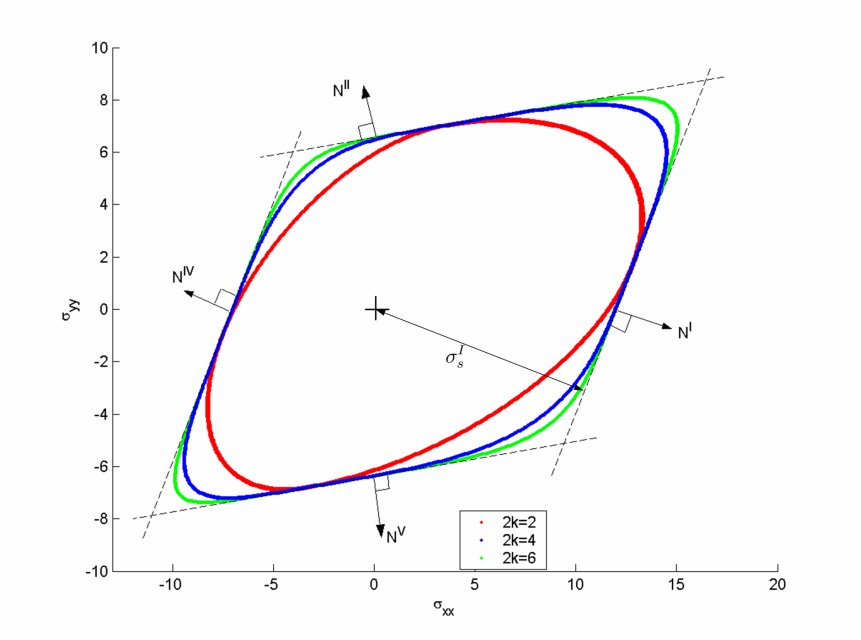

Figure 3.2: Yield surface with different k-values with the remaining parameters set for the mechanical ply proposed by Xia (2002), and $\sigma_{xy} = 0$.

$$\chi_I = \begin{cases} 1 & \text{if } \boldsymbol{\sigma} : \mathbf{N}_I > 0; \\ 0 & \text{otherwise.} \end{cases} \tag{3.17}$$

In the model, the size of the yield surface is controlled by one parameter, namely the effective plastic strain ε_{eff}^p defined in the next section. Figure 3.3 shows how the yield surface evolves with the plastic strain, when the hardening parameters for the mechanical ply proposed by Xia (2002) is used.

3.2.2 Flow rule

Once the yield surface is reached the material starts to flow, and plasticity develops. The direction of the flow is in the model perpendicular to the yield surface

$$\hat{\mathbf{K}} = \frac{\partial f}{\partial \boldsymbol{\sigma}}. \tag{3.18}$$

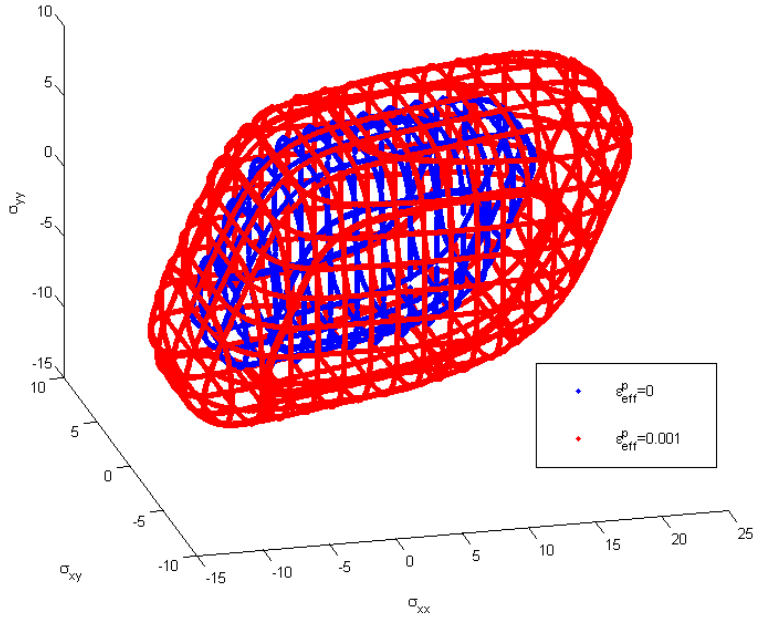

Figure 3.3: Yield surface at different ε^p_{eff} with parameters for the mechanical ply proposed by Xia (2002).

Hence the flow is associated. The flow is normalised to give a magnitude of one unit in the flow direction $\mathbf{K}$,

$$\mathbf{K} = \frac{\hat{\mathbf{K}}}{\left\|\hat{\mathbf{K}}\right\|}. \tag{3.19}$$

The rate of the plastic flow[1] is

$$\dot{\boldsymbol{\varepsilon}}^p = \dot{\lambda}\mathbf{K}, \tag{3.20}$$

where λ is the plastic multiplier[2]. When determining the normal directions ($\boldsymbol{N}$) to the sub-surfaces in the yield criterion, use is made of the fact that we have associate flow and the assumption that only one yields surface is active[3] for uniaxial tension, uniaxial compression and pure shear. In this way the direction of plastic flow in uniaxial tests coincide with $\boldsymbol{N}$.

To give a short idea how $\boldsymbol{N}$ is calculated we consider uniaxial MD tension and calculate

[1]It should be noted that the model is statical, no dynamical effects or time dependencies occur. The denominator dt in for example $\dot{\lambda} = \frac{d\lambda}{dt}$ can be cancelled out and give the incremental form $d\lambda$. The incremental form shows a change in property rather than a change in time. This is a convenient and widely used notation.

[2]The plastic multiplier can be compared with the Lagrange multiplier that shows up in more general cases outside the solid mechanics.

[3]The assumption that only one sub-surface is active is not strictly true as can be seen in figure 3.2, but for high values of k this is a reasonable assumption.

the normal direction to the corresponding sub-surface ($\boldsymbol{N}^I$). It is assumed that there is no shear strain when paperboard is loaded in MD tension according to equation (3.14), which gives $N^I_{MD,CD} = 0$. By considering the symmetry in the papermaking process it can be concluded that this is a reasonable assumption. In figure 3.4 it is seen that the plastic strain ratio ($\frac{d\varepsilon^p_{CD}}{d\varepsilon^p_{MD}}$) is almost constant at -0.5 (Xia, 2002). From this the two remaining direction components are calculated according to

$$\frac{(N_{CD})^I}{(N_{MD})^I} = -0.5 \tag{3.21}$$

and (to make a unit normal)

$$((N_{MD})^I)^2 + ((N_{CD})^I)^2 = 1. \tag{3.22}$$

This gives $(N_{MD})^I = 2/\sqrt{5}$ and $(N_{CD})^I = -1/\sqrt{5}$. For CD tension experiments (Xia, 2002) show that the plastic strain ratio is around $-2/15$ and the sub-surface corresponding to CD tension N_{II} can be calculated with the same approach. The remaining sub-surfaces can be calculated in the same fashion. However, currently, there is no experimental data for plastic strain ratios in compression therefore the normals to the sub-surfaces corresponding to compression is assumed to be antiparallel to those of the corresponding tensile normal. In pure shear the normal stress components is not active according to equation (3.14) and the normal is set with the magnitude of one unit and to point out from the yield surface. The directions for the normals to the sub-surfaces is summarized in table 5.3.

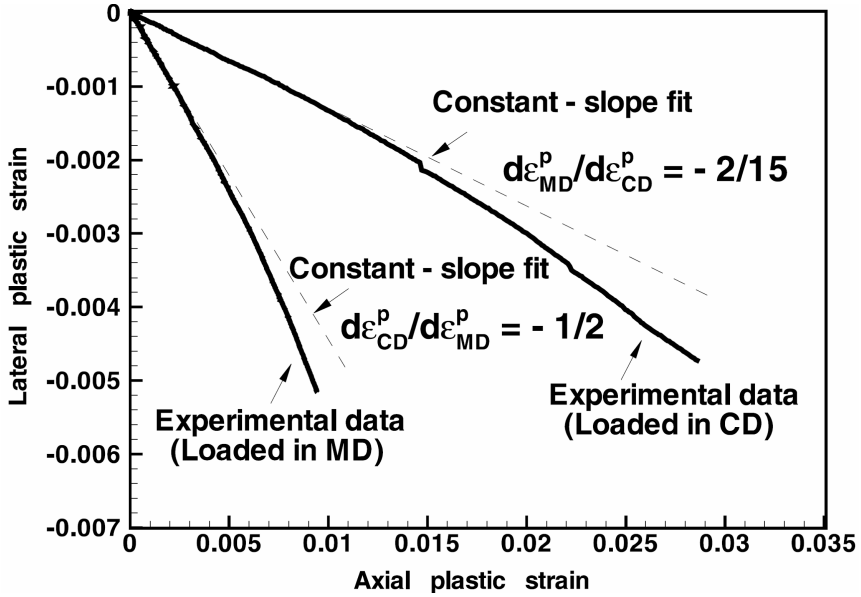

Figure 3.4: Lateral plastic strain vs. axial plastic strain curves for tensile loading in the MD and CD directions. Adopted from Xia (2002).

3.2.3 Hardening

The hardening of the in-plane model is captured with the parameters that determine the size of the yield surface (σ_s^I). These parameters evolve with the effective plastic strain, ε_{eff}^p. It is assumed that the yield planes harden according to

$$\sigma_s^I = \sigma_{s0}^I + A_1 tanh(B_1\varepsilon_{eff}^p) + C_1\varepsilon_{eff}^p, \tag{3.23}$$
$$\sigma_s^{II} = \sigma_{s0}^{II} + A_2 tanh(B_2\varepsilon_{eff}^p) + C_2\varepsilon_{eff}^p, \tag{3.24}$$
$$\sigma_s^{III} = \sigma_{s0}^{III} + A_3 tanh(B_3\varepsilon_{eff}^p) + C_3\varepsilon_{eff}^p, \tag{3.25}$$
$$\sigma_s^{IV} = \sigma_{s0}^{IV} + A_4 tanh(B_4\varepsilon_{eff}^p) + C_4\varepsilon_{eff}^p, \tag{3.26}$$
$$\sigma_s^{V} = \sigma_{s0}^{V} + A_5 tanh(B_5\varepsilon_{eff}^p) + C_5\varepsilon_{eff}^p, \tag{3.27}$$
$$\sigma_s^{VI} = \sigma_s^{III}(\varepsilon_{eff}^p), \tag{3.28}$$

where ε_{eff}^p is the effective plastic strain and is defined as

$$\varepsilon_{eff}^p = \sqrt{{\varepsilon_{xx}^p}^2 + {\varepsilon_{yy}^p}^2 + \frac{{\gamma_{xy}^p}^2}{2}}. \tag{3.29}$$

This can seem an odd way of defining the effective plastic strain, but comes from the fact that we use engineering shear strain and a vector with three components. This can be done since the stress and strain tensor used by Xia (2002) is symmetric and that only three components are used in the in-plane yield criterion.

3.3 Out-of-plane model

The continuum model presented by Xia (2002) does not include plastic behaviour in the out-of-plane components. However, the importance of adding an elasto-plastic constitutive law into these components has been recognized, cf. section 2.2.2.

The behaviour of paperboard in ZD compression and the shear behaviour in the delamination planes has been examined by Stenberg (2002b). In addition, a model for the out-of-plane components, to be combined with the interface model proposed by Xia (2002), has been proposed by Stenberg (2003). Within the scope of this work this model has been implemented. However, the formulation causes two problems:

1. It causes a discontinuity in ZD-compression and is therefore not suitable for numerical methods.
2. It does not capture the relevant behaviour in shear.

More details about this in appendix A.

A new model for the out-of-plane components is proposed in this chapter. The model relates the stress

$$\boldsymbol{\sigma} = \begin{bmatrix} \sigma_{zz} \\ \tau_{xz} \\ \tau_{yz} \end{bmatrix} \quad \text{and the strain} \quad \boldsymbol{\varepsilon} = \begin{bmatrix} \varepsilon_{zz} \\ 2\varepsilon_{xz} \\ 2\varepsilon_{yz} \end{bmatrix} = \begin{bmatrix} \varepsilon_{zz} \\ \gamma_{xz} \\ \gamma_{yz} \end{bmatrix}. \tag{3.30}$$

In the model the behaviour in ZD compression relies on experimental data presented by Stenberg (2002b), cf. figure 2.6(a). Paper shows a nonlinear elastic behaviour in ZD compression. The elastic stiffness, E_{zz}, depends both upon the elastic strain and the plastic strain, hence

$$E_z = E_z(\varepsilon^e_{zz}, \varepsilon^p_{zz}). \tag{3.31}$$

The behaviour of the out-of-plane shear components are more problematic than the ZD compression. To the knowledge of the author the out-of-plane shear relevant for the continuum model has not been experimentally examined. It involves great difficulties to measure this behaviour mainly because of two reasons; during the experiments no delamination of the paper is allowed to occur since the interface model should capture this behaviour; the small thickness of the paper leads to significant problem when measuring the shear. Therefore, a trial and error procedure with an application which exposes the paper for out-of-plane shear is needed to calibrate the model. Hence, the model proposed for the shear model is a simple model with few parameters that need to be determined.

3.3.1 ZD compression

As earlier the total strain is divided in an elastic and a plastic part,

$$\varepsilon = \varepsilon^e + \varepsilon^p. \tag{3.32}$$

In this model the paper will be treated as a porous material and the elastic deformation of the paper will consist of deformation on the solid fibre structure, ${}^{sol}\varepsilon^e$, and deformation of the voids, ${}^{void}\varepsilon^e$.

$$\varepsilon^e = {}^{void}\varepsilon^e + {}^{sol}\varepsilon^e \tag{3.33}$$

To characterise the material the void ratio, r, is used

$$r = \frac{{}^{void}V}{{}^{sol}V}, \tag{3.34}$$

where ${}^{void}V$ is the volume of the voids and ${}^{sol}V$ is the volume of the solid fibres.

For porous materials the stress and the strain are often split in two invariants, the deviatoric and the hydrostatic. It is experimentally observed that during elastic deformation of porous materials the change in void ratio and the change in the logarithm of the hydrostatic pressure is linearly related (ABAQUS, 2004). This gives the relation

$$dr^e = -\mu d(ln(p + p_t)), \tag{3.35}$$

where μ is a material parameter, p is the equivalent hydrostatic pressure defined as

$$p = \frac{1}{3}\sigma_{ij}\delta_{ij} \tag{3.36}$$

and p_t is the hydrostatical tensile strength (defined positive in tension), $p + p_t > 0$.

Since paper is highly anisotropic, with the stiffness in ZD being far less than the in-plane stiffness, the split of the stress in a deviatoric and a volumetric part is not believed to be of interest. Because of the anisotropy the out-of-plane normal stress component, σ_{zz}, is significantly more important to the void ratio than the in-plane normal stress components (shear stress does not influence the volume in orthotropic materials when small deformations are considered and therefore neither the void ratio). The in-plane strain components are also small when the paper breaks, and the assumption that in-plane stresses does not influence the void ratio is made. With this assumption equation (3.34) takes the form

$$r = \frac{^{void}t}{^{sol}t} \tag{3.37}$$

where ^{void}t is the mean value of the thickness of the voids in ZD over a point, and ^{sol}t is the mean value of the thickness of the solid in ZD.

In the following the *orig* subscript relates to the original paper where no deformation has occurred. With geometrical considerations and the definition of true strain

$$\begin{cases} ^{void}t_{orig} + ^{sol}t_{orig} = t_{orig} \\ ^{void}t + ^{sol}t = t \\ r = \frac{^{void}t}{^{sol}t} \\ r_{orig} = \frac{^{void}t_{orig}}{^{sol}t_{orig}} \\ \varepsilon_{zz} = ln\frac{t}{t_{orig}} \end{cases} \tag{3.38}$$

and by neglecting the compressibility of the solid material, $^{sol}t_{orig} = ^{sol}t$, we get

$$\varepsilon_{zz} = ln(\frac{1+r}{1+r_{orig}}), \tag{3.39}$$

rearrangement yields

$$r = (r_{orig}+1)e^{\varepsilon_{zz}} - 1 = (r_{orig}+1)e^{\varepsilon^e_{zz}}e^{\varepsilon^p_{zz}} - 1. \tag{3.40}$$

We now introduce r_0 as the void ratio when the elastic deformation has been relaxed,

$$r_0 = (r_{orig}+1)e^{\varepsilon^p_{zz}} - 1. \tag{3.41}$$

In the following the subscript 0 relates to the state when the material is relaxed so that there is no elastic deformation. In the same manner as earlier, but now considering the

elastic strain, we have

$$\begin{cases} {}^{void}t^e + {}^{sol}t^e = t^e \\ {}^{void}t_0 + {}^{sol}t_0 = t_0 \\ r_0 = \frac{{}^{void}t_0}{{}^{sol}t_0} \\ r^e = \frac{{}^{void}t^e}{{}^{sol}t^e} \\ \varepsilon^e_{zz} = ln\frac{t^e}{t_0} \\ {}^{sol}t_0 = {}^{sol}t^e \end{cases} \tag{3.42}$$

which gives

$$\varepsilon^e_{zz} = ln(\frac{1+r^e}{1+r_0}), \tag{3.43}$$

rearrangement yields

$$r^e = (r_0+1)e^{\varepsilon^e_{zz}} - 1. \tag{3.44}$$

The assumption that the in-plane stress components does not influence the void ratio make equation (3.35) take the form

$$dr^e = -\mu d(ln(-\frac{1}{3}\sigma_{zz} + \frac{1}{3}\sigma^t_{zz})), \tag{3.45}$$

Integration of equation (3.45) yields

$$\sigma_{zz} = Ae^{\left(-\frac{1}{\mu}r^e\right)} + \sigma^t_z, \tag{3.46}$$

where A is a constant and σ^t_{zz} is the strength in tension. The constant A is defined according to the boundary condition $\sigma_{zz} = 0 \Rightarrow \varepsilon^e_{zz} = 0$ and equation (3.46) takes the form

$$\sigma_{zz} = \sigma^t_z(1 - e^{\frac{1}{\mu}(r_0 - r^e)}), \tag{3.47}$$

with r_0 and r^e defined in equation 3.44 and equation 3.41 and $\varepsilon^e_{zz} = \varepsilon_{zz} - \varepsilon^p_{zz}$ from equation 3.32, we get

$$\sigma_{zz} = \sigma^t_z\left(1 - exp\left[\frac{1+r_{orig}}{\mu}(exp[\varepsilon^p_{zz}] - exp[\varepsilon_{zz}])\right]\right) \tag{3.48}$$

Yield criterion

As in the in-plane model a yield function $f(\sigma_{zz}, \varepsilon^p_{zz})$ governs whether or not plastic deformation occurs. The model has only plasticity in compression since it is assumed that the interface model takes care of the delamination in ZD tension. In tension of the continuum model the function reaches the tensile yield stress, σ^t_z asymptotically. The sign of the function $f(\sigma_{zz}, \varepsilon^p_{zz})$ is chosen such that $f(\sigma_{zz}, \varepsilon^p_{zz}) < 0 \rightarrow$ elastic behaviour. Hence,

$$f = \sigma_s(\varepsilon^p_{zz}) - \sigma_{zz} = 0 \tag{3.49}$$

where σ_s is the yield stress in ZD compression.

Flow rule

An associate flow is chosen such that

$$\dot{\varepsilon}^p_{zz} = \dot{\lambda}\frac{\partial f}{\partial \sigma_{zz}}. \tag{3.50}$$

If use is made of the fact that there is only plasticity in compression equation 3.50 becomes

$$\dot{\varepsilon}^p_{zz} = -\dot{\lambda} \tag{3.51}$$

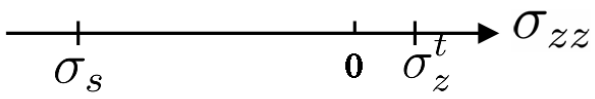

Figure 3.5: Yield criterion for out-of-plane compression.

Hardening

The hardening parameter σ_s is proposed to follow

$$\sigma_s = A_\sigma + B_\sigma e^{(-C_\sigma \varepsilon^p_{zz})} \tag{3.52}$$

3.3.2 Out-of-plane shear

In this section an elasto-plastic out-of-plane shear behaviour is proposed. An elasto-plastic shear model is of importance to a simulation like creasing, but as mentioned earlier this behaviour is hard to investigate experimentally. Therefore, the model proposed is a simple model and should, if necessary, be extended when experimental data are available.

Yield criterion

The yield surface relates the effective shear stress to the yield stress (τ_s), hence the yield surface is circular in a σ_{xz}/σ_{yz}-coordinate system with the yield stress as radial distance, cf. figure 3.6. Accordingly,

$$f = \sqrt{\sigma^2_{xz} + \sigma^2_{yz}} - \tau_s. \tag{3.53}$$

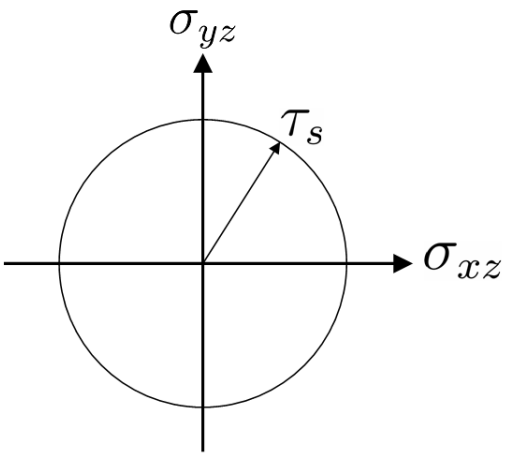

Figure 3.6: Yield criterion for out-of-plane shear. τ_s is the radius of the circle.

Hardening

The hardening is controlled by the yield stress that evolves with the plastic strain according to

$$\tau_s = A_\tau + B_\tau tanh(C_\tau \gamma^p_{eff}) \tag{3.54}$$

where γ^p_{eff} is defined as the magnitude of the plastic out-of-plane engineering shear strain, hence

$$\gamma^p_{eff} = \|\gamma^p\| \,. \tag{3.55}$$

Flow rule

The plastic flow evolves with an associate flow rule,

$$\dot{\gamma}^p = \dot{\lambda} \frac{\partial f / \partial \boldsymbol{\sigma}}{\|\partial f / \partial \boldsymbol{\sigma}\|}. \tag{3.56}$$

Chapter 4

Implementation

As mentioned earlier we are interested in the response of paper when loads and displacements are applied, in other words we are interested in solving boundary value problems. The constitutive equations and in general the geometries are far too complex to solve with an exact analytical approach. Therefore an approximate numerical method is needed. Today, the most widely used and most powerful method is the finite element (FE) method.

The FE method is a numerical approach that is used to solve differential equations over a field. Field problems are common when modelling physical phenomena, e.g. all kinds of flow like heat flux, diffusion, gas flow, liquid flow and electrical flow, and others like wave propagation and vibration. In the FE method the fields are divided in small parts, finite elements. The variable to solve for is then approximated with simple (e.g. linear) functions over the elements. In this way we get many simple equations to solve which is suitable for today's computers. The FE method builds on the, for engineers, very useful principle of virtual work and the weak formulation of the differential equations. For further knowledge on the FE method consult Zienkiewicz and Taylor (2000) or Ottosen and Petersson (1992).

There are mainly two groups of FE-programs: Implicit and Explicit. An implicit program, as opposed to an explicit program, iterates until equilibrium (force equilibrium in our case) is achieved in every node point in every increment. In this chapter the implementation of the constitutive models into a FE-program is described. Since the model is implemented into an implicit program focus will be addressed to this method.

A nonlinear implicit FE problem is composed of two subsets: solution of the global equilibrium equation and integration of the constitutive equations in every material point (i.e. every Gauss point). These equations are trivial in the linear FE method, but not in the nonlinear FE method. If the response of the material is nonlinear and not all nodes are prescribed the solver needs to iterate over the material model and the kinematics according to figure 4.1. In the following two sections one method to solve these equations is presented, there are more methods to use, for further knowledge consult Ottosen and Ristinmaa (2005) or Belytschko et al. (2000).

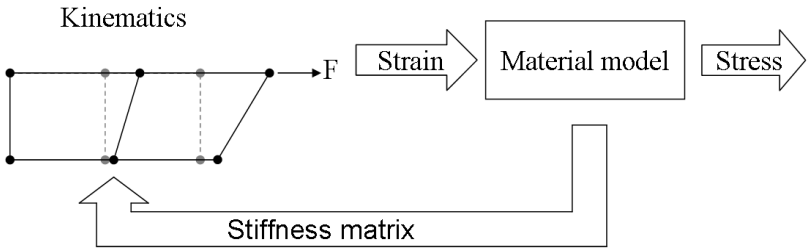

Figure 4.1: Principle for the role of the material model. F is a force applied.

4.1 Solution of equilibrium equation

For a static problem the global equilibrium equation to solve is

$$\boldsymbol{\Psi}(\boldsymbol{a}) = 0, \tag{4.1}$$

where $\boldsymbol{\Psi}$ is the out-of-balance forces and $\boldsymbol{a}$ refer to the displacements of the nodes, with the number of components equal to the degrees of freedom in the structure (nodes×degrees of freedom at every node). $\boldsymbol{\Psi}$ is defined as

$$\boldsymbol{\Psi} = \boldsymbol{f}_{int} - \boldsymbol{f}, \tag{4.2}$$

where $\boldsymbol{f}$ is the external forces applied to the nodes of the structure. $\boldsymbol{f}_{int}$ denotes the internal forces that the stress, $\boldsymbol{\sigma}$, causes. The internal stress is dependent on the material behaviour that will be examined in the next section. There are different ways of solving the global equilibrium equations; ABAQUS/Standard uses a Newton-Raphson approach. Figure 4.2 shows the principle of this approach when using it to solve equilibrium equations. Since the response of the structure is nonlinear and the response is history dependent the forces in general need to be applied stepwise, in small increments[1]. The subscript n refers to the beginning of the increment i.e. a known state, and the subscript $n+1$ refers to the end of the increment, where only the new increment of external forces is known. The superscript i refers to the load iterations. By knowing the stiffness from the last iteration a new displacement can be calculated according to

$$\boldsymbol{K}_t^{i-1}(\boldsymbol{a}^i - \boldsymbol{a}^{i-1}) = \boldsymbol{f}_{n+1} - \boldsymbol{f}_{int}^{i-1}. \tag{4.3}$$

The variable $\boldsymbol{K}_t$ is described differently depending on the method used. In a Newton-Raphson approach $\boldsymbol{K}_t$ is the material tangent stiffness, $\boldsymbol{\mathcal{L}}^{ATS}$, updated in every load iteration, hence

$$\boldsymbol{K}_t = \boldsymbol{\mathcal{L}}^{ATS}. \tag{4.4}$$

[1] In general numerical methods this is sometimes referred to as the homotopy method.

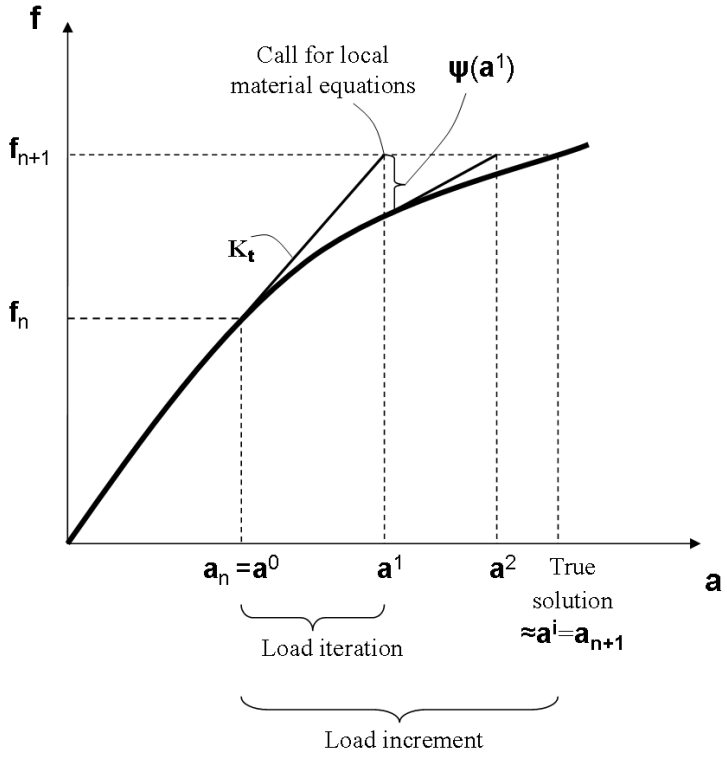

Figure 4.2: Principle of the Newton-Raphson scheme used in the global equilibrium iterations.

Sometimes it is computationally efficient to update $\boldsymbol{K}_t$ more seldom, this is referred to as a modified Newton-Raphson method. How the material tangent stiffness, $\boldsymbol{\mathcal{L}}^{ATS}$, is calculated is described in section 4.3.

When the displacements, $\boldsymbol{a}$, are known the strains $\boldsymbol{\varepsilon}$ can be calculated and we call for the solution of the local material model to integrate the stress, $\boldsymbol{\sigma}$, and from this calculate the new internal forces acting on the nodes. When the displacements are corrected, such that the out-of-balance forces are sufficiently close to zero, the solution is reached. In table 4.1 the Newton-Raphson scheme used to solve the global equilibrium equation is outlined, this is mainly to give the main idea, for the specific equations consult Ottosen and Ristinmaa (2005).

The Newton-Raphson method is commonly used in all kinds of numerical methods since the convergence rate is fast. The Newton-Raphson method reaches quadratic convergence when the Jacobian used is correctly derived. This means that the number of correct digits in the answer roughly doubles in every iteration. A more strict way of defining convergence rate is

$$\lim_i \frac{|x_{i+1} - \xi|}{|x_i - \xi|^q} = \mu \text{ with } \mu > 0, \tag{4.5}$$

Table 4.1: The Newton-Raphson approach applied to solve equilibrium equations.

- Call local material model with zero load to get initial stiffness.
- For load increment $n = 0, 1, .., N_{end}$.
  - Determine new load level $\boldsymbol{f}_{n+1}$.
  - Iterate until $\boldsymbol{\psi}(\boldsymbol{a})_{norm} < tolerance$.
    - Calculate $\boldsymbol{a}^1$ from $\boldsymbol{K}^{i-1}(a^i - a^{i-1}) = \boldsymbol{f}_{n+1} - \boldsymbol{f}_{int}^{i-1}$.
    - Calculate ε^i with a^i and the shape functions[a].
    - Call local material model to get $\boldsymbol{\sigma}^i$ and material stiffness at each Gauss point (see following section).
    - Assemble the global stiffness matrix $\boldsymbol{K}_t$, depending on material stiffnesses and topology data.
    - Integrate internal forces $\boldsymbol{f}_{int}^i$ from the stresses.
  - End iteration loop.
  - Accept quantities.
- End load step loop.

[a]For further knowledge on shape functions consult Ottosen and Petersson (1992)

where $\{x_i\}$ is the sequence that converges towards the solution ξ, i is the iteration, μ the rate of convergence and q the order of the convergence. Convergence with $q = 2$ is called quadratic convergence.

However, the Newton-Raphson method has a drawback; the tangent stiffness has to be non-singular for the method to converge, i.e.

$$\det K_t \neq 0. \tag{4.6}$$

This restriction causes problems when dealing with softening material since $det(K_t) = 0$ at peak loads, when $\dot{a} \neq 0$ and $\dot{f} = 0$. There are different ways of handling this but since we do not encounter these kinds of problems these methods will not be explained, the interested reader may consult Ottosen and Ristinmaa (2005).

4.2 Integration of constitutive equations

In the previous section it was mentioned that the internal forces $\boldsymbol{f}_{int}$ depend on the stresses $\boldsymbol{\sigma}$ which depend on the constitutive equations. In this section we will see how this is calculated. This part is what the user needs to implement when implementing a material model. As can be seen in figure 4.2 the nodal displacements are fixed and therefore the strains are fixed and the stresses need to be calculated in order to be able to calculate the internal forces in the global equations. First we check if the increment is elastic or plastic.

This is done by assuming that the increment is elastic and calculating the trial stress $\boldsymbol{\sigma}^\star$ defined as

$$\boldsymbol{\sigma}^\star = \boldsymbol{\sigma}_{(n)} + \boldsymbol{D}(\boldsymbol{\varepsilon}^{(i)} - \boldsymbol{\varepsilon}_{(n)}) \tag{4.7}$$

If the trial stress is inside the yield surface the assumption was correct and the trial stress is the correct stress at the end of the iteration. If the trial stress is outside the yield surface the assumption was wrong and part of, or the entire iteration step, was plastic. To find out the new stress the integral

$$\boldsymbol{\sigma}^{(i)} = \boldsymbol{\sigma}_{(n)} + \int_{(n)}^{(i)} \boldsymbol{D} d\boldsymbol{\varepsilon} \tag{4.8}$$

needs to be derived, where n refers to the state at the beginning of the increment where everything is known and i refers to the state where only $\boldsymbol{\varepsilon}$ is known, provided from the global FE equations. Note that the integration limits is between the state when equilibrium last was achieved to the present load integration, cf. figure 4.2.

If we have a flow rule defined in rate form, the constitutive equations need to be studied at incremental level when plasticity starts to develop according to

$$\dot{\boldsymbol{\sigma}} = \boldsymbol{D} \cdot \left(\dot{\boldsymbol{\varepsilon}} - \dot{\boldsymbol{\varepsilon}^p}\right). \tag{4.9}$$

This together with an associated flow rule, $\dot{\boldsymbol{\varepsilon}^p} = \dot{\lambda}\frac{\partial f}{\partial \boldsymbol{\sigma}}$, and by studying the equations stepwise, as is done in numerical solutions, we get

$$\Delta\boldsymbol{\sigma} = \boldsymbol{D} \cdot \left(\Delta\boldsymbol{\varepsilon} - \Delta\lambda\frac{\partial f}{\partial \boldsymbol{\sigma}}\right) \tag{4.10}$$

where Δ refer to the difference in quantity between state i and state n (i.e. $\Delta x = x^i - x_n$). Equation 4.10 together with 4.7 gives

$$\sigma_i^{(i)} = \sigma_i^\star - D_{ik}\Delta\lambda\frac{\partial f}{\partial \sigma_k}. \tag{4.11}$$

If the flow direction is normalized, as in our constitutive equations,

$$\Delta\lambda = \Delta\varepsilon_{eff}. \tag{4.12}$$

In equation (4.11) the unknown components are the stress ($\boldsymbol{\sigma}$) and the increment of the plastic multiplier ($\Delta\lambda$), but the equation is only as many as the stress components, therefore one more equation is needed. It is a fundamental statement in plasticity theory that we never leave the yield surface. We are at the edge of the yield surface when plasticity develops and the yield surface expands with strain hardening (or contracts if the material softens). This gives the relation

$$f = 0 \tag{4.13}$$

that can be achieved mainly by two methods. Directly by saying that $f = 0$, which is referred to as the direct method. Alternatively by saying that the derivative $\dot{f} = 0$ which

is referred to as the indirect method. We will make use of the direct method. We now have enough equations to solve the unknown components. The only remaining part is to define where to calculate the flow direction $\frac{\partial f}{\partial \boldsymbol{\sigma}}$. This can be done at $\boldsymbol{\sigma}^{(i)}$, $\boldsymbol{\sigma}_{(n)}$ or anywhere between the two. Here we calculate the flow direction at the end of the increment,$\boldsymbol{\sigma}_{(n)}$, which is referred to as a fully implicit scheme or an Euler backward method. The fully implicit scheme has the advantages that it is always stable cf. Ortiz and Popov (1985) and that it is accurate cf. Ottosen and Ristinmaa (2005). To sum up the equations which need to be solved we have

$$\boldsymbol{\mathcal{F}} = \begin{bmatrix} \sigma_i^{(i)} - \sigma_i^{\star} + D_{ik}\Delta\lambda \frac{\partial f}{\partial \sigma_k^{(i)}} \\ f(\boldsymbol{\sigma}^{(i)}, \Delta\lambda) \end{bmatrix} = \mathbf{0} \tag{4.14}$$

with the unknown components

$$\boldsymbol{x} = \begin{bmatrix} \Delta\lambda \\ \sigma_i^{(i)} \end{bmatrix}. \tag{4.15}$$

In figure 4.3 equation 4.14 is illustrated. This method is usually referred to as a return

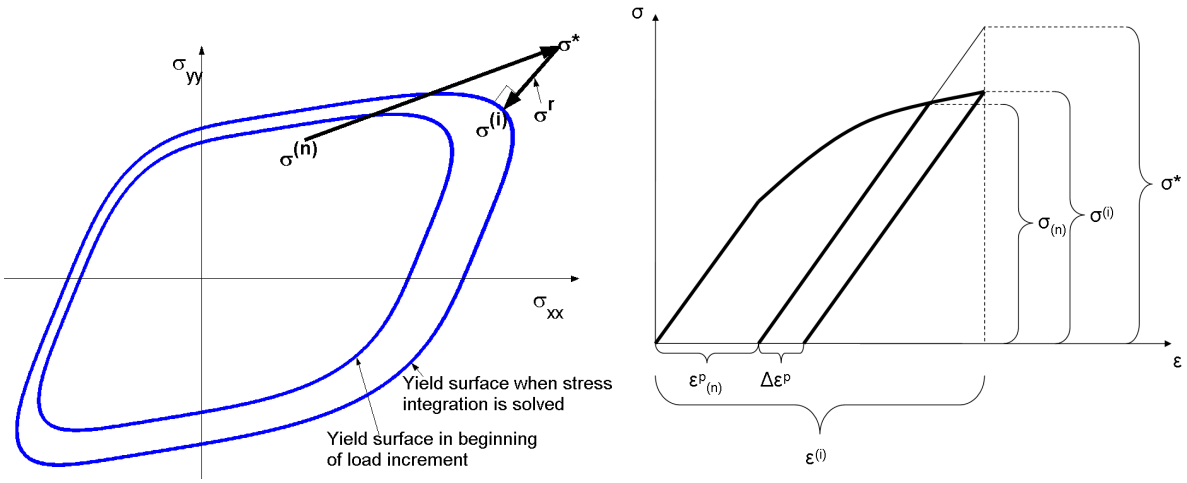

(a) Illustration of the return method with two stress components.

(b) Illustration of the return method with one stress component.

Figure 4.3: Return method

method[2] since we have a return stress $\boldsymbol{\sigma}^r$ that is used to return to the yield surface according to

$$\boldsymbol{\sigma}^i = \boldsymbol{\sigma}^{\star} + \boldsymbol{\sigma}^r, \tag{4.16}$$

where $\boldsymbol{\sigma}^r$ is the return stress, defined - according to the method we used - as

$$\boldsymbol{\sigma}^r = -D_{ik}\Delta\lambda \frac{\partial f}{\partial \sigma_k^{(i)}}. \tag{4.17}$$

[2]When return methods are discussed it can seem like we have left the yield surface; this is just in the implementation and to some extent imaginary.

The return method is illustrated in figure 4.3. In the implementation the equation (4.14) is solved with the Newton-Raphson method

$$\boldsymbol{x}_{(s+1)} = \boldsymbol{x}_{(s)} - \left(\frac{d\boldsymbol{\mathcal{F}}}{d\boldsymbol{x}}\right)^{-1}_{(s)} \boldsymbol{\mathcal{F}}_{(s)}. \tag{4.18}$$

The Jacobian $\frac{d\boldsymbol{\mathcal{F}}}{d\boldsymbol{x}}$ in equation (4.18) is derived, for our specific model, in appendix B. This Jacobian is also used in the calculation of the material stiffness matrix as we will see in the next section.

4.3 Material tangent stiffness matrix

In this section the material tangent stiffness $\boldsymbol{\mathcal{L}}^{ATS}$ as can be seen in figure 4.2 is derived. The tangent stiffness is of vital importance when using a Newton-Raphson approach in order to get a satisfying convergence rate. An incorrect calculation of the tangent stiffness matrix only influences the convergence rate, the result (if obtained) is unaffected. The tangent stiffness is defined as

$$\boldsymbol{\mathcal{L}}^{ATS} = \frac{d\boldsymbol{\sigma}}{d\boldsymbol{\varepsilon}}. \tag{4.19}$$

If the response of the material is elastic the matrix is the elastic tangent stiffness $\boldsymbol{D}$. When the response is plastic the stiffness matrix depends both upon the material model and the way that it is integrated (therefore it is sometimes called consistent stiffness matrix since it has to be consistent with the integration method). When equation 4.14 is solved and the values are updated we have

$$\boldsymbol{\mathcal{F}}(\Delta\lambda, \boldsymbol{\sigma}, \boldsymbol{\varepsilon}) = \boldsymbol{0}. \tag{4.20}$$

$\boldsymbol{\mathcal{F}}$ can be rewritten as

$$\boldsymbol{\mathcal{F}}(\boldsymbol{x}, \boldsymbol{\varepsilon}), \tag{4.21}$$

with $\boldsymbol{x}$ containing $\Delta\lambda$ and $\boldsymbol{\sigma}$. Linearization yields

$$\frac{\partial\boldsymbol{\mathcal{F}}}{\partial\boldsymbol{x}} d\boldsymbol{x} + \frac{\partial\boldsymbol{\mathcal{F}}}{\partial\boldsymbol{\varepsilon}} d\boldsymbol{\varepsilon} = \boldsymbol{0} \tag{4.22}$$

which gives

$$\frac{d\boldsymbol{x}}{d\boldsymbol{\varepsilon}} = -\left(\frac{\partial\boldsymbol{\mathcal{F}}}{\partial\boldsymbol{x}}\right)^{-1} \frac{\partial\boldsymbol{\mathcal{F}}}{\partial\boldsymbol{\varepsilon}}, \tag{4.23}$$

with $\frac{\partial\boldsymbol{\mathcal{F}}}{\partial\boldsymbol{x}}$ being the same matrix as in equation (4.18) when the solution is found (i.e. $\boldsymbol{\mathcal{F}}$ is sufficient close to zero). $\frac{d\boldsymbol{x}}{d\boldsymbol{\varepsilon}}$ contains the sought material stiffness, $\frac{d\boldsymbol{\sigma}}{d\boldsymbol{\varepsilon}}$.

In appendix B the material stiffness matrix is calculated for our specific model.

4.4 ABAQUS/Standard

The model has first been implemented into CALFEM (Compute Aided Learning of the Finite Element Method) which is a toolbox for MATLAB developed in order to teach the FE-method (Austrell et al., 2004). With CALFEM an FE program can more easily be built than from scratch. In MATLAB it is checked that quadratic convergence is achieved both when the outer global equations and the inner constitutive equations are solved. This is done to be sure that the correct Jacobians are derived. The model is then implemented into the implicit finite element program ABAQUS/Standard using the programming language Fortran 90. ABAQUS/Standard uses the Newton-Raphson approach which is outlined in section 4.1.

The solution procedure for the global equations does not depend on the constitutive models. Therefore this part can be implemented with a general solution technique that works for arbitrary material model. ABAQUS/Standard takes care of this part, and in order to get a working material model the constitutive equations need to be integrated and the material stiffness needs to be calculated.

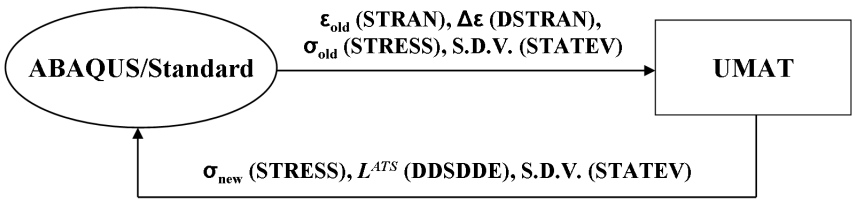

Figure 4.4: Interaction between ABAQUS/Standard and UMAT.

The model has been implemented as a user defined subroutine, UMAT (User-defined mechanical material). The UMAT is called for at each material point (i.e. gauss point) at each iteration of every increment. The interaction between ABAQUS/Standard and the UMAT is described in figure 4.4. The basic idea is that ABAQUS/Standard delivers the material state at the start of the increment and the difference in strain between old state and new state ($\Delta\varepsilon$). The state in the start of the increment is described by the old stress (in the variable STRESS), the old strain (in the variable STRAN), and the solution-dependent state variables (in the variable STATEV). The solution-dependent state variables are defined by the user and are in our case the three state variables coupled to the plastic strain that describes the state of the yield surfaces. The purpose of the UMAT is to calculate and return the stress and the solution-dependent state variables at the end of the increment. Furthermore the UMAT needs to provide the material tangent stiffness (in the variable DDSDDE).

The current version of the UMAT, smallpapermodel1.f, has the three solution dependent state variables stated in table 4.2. The properties given as input to the UMAT is described

in table 4.3. The uncontinuous numbering of the input properties is because we want to use the same properties card as for the current implemented 3DM model version 3.3 (Nygårds, 2005). In the present version of the UMAT the gradients to the yield planes ($\boldsymbol{N}$) has to be changed in the Fortran-file and the exponent in the yield condition ($2k$) is currently (unfortunately) part of the equations. These parameters are currently set as the values in table 5.1. The directions in the UMAT are defined in the same manner as in the 3DM implementation; with axis 1 for MD, axis 2 for ZD and axis 3 for CD.

Table 4.2: Solution dependent variables.

SDV #s	Notation	Description
SDV(1)	ε^p_{zz}	Plastic strain in ZD compression.
SDV(2)	γ^p_{eff}	Effective strain in out-of-plane shear.
SDV(3)	ε^p_{eff}	Effective strain in in-plane model.

Table 4.3: Input parameters for the continuum model

Prop.	Notation	Description
1	E_x	Elastic modulus in MD /MPa
3	E_y	Elastic modulus in CD /MPa
4	ν_{xy}	In-plane Poisson's ratio (ν_{yx} is calculated from equation (3.11))
6	G_{xy}	In-plane shear modulus /MPa
11	σ_1^0	Parameter for initial tensile yield plane in MD /MPa
12	σ_2^0	Parameter for initial tensile yield plane in CD /MPa
13	σ_3^0	141.4% of initial yield stress in pure shear /MPa
14	σ_4^0	Parameter for initial compression yield plane in MD /MPa
15	σ_5^0	Parameter for initial compression yield plane in CD /MPa
16	A_1	Hardening parameter /MPa
17	A_2	Hardening parameter /MPa
18	A_3	Hardening parameter /MPa
19	A_4	Hardening parameter /MPa
20	A_5	Hardening parameter /MPa
21	B_1	Hardening parameter
22	B_2	Hardening parameter
23	B_3	Hardening parameter
24	B_4	Hardening parameter
25	B_5	Hardening parameter
26	C_1	Hardening parameter
27	C_2	Hardening parameter
28	C_3	Hardening parameter
29	C_4	Hardening parameter
30	C_5	Hardening parameter
34	μ	Parameter for elastic behaviour in ZD
35	r_{orig}	Initial void ratio
36	σ_z^t	Strength in ZD tension /MPa
37	A_σ	Hardening parameter for ZD compression /MPa
38	B_σ	Hardening parameter for ZD compression /MPa
39	C_σ	Hardening parameter for ZD compression
40	$G_{xz} = G_{yz}$	Shear modulus in out-of-plane shear /MPa
41	A_τ	Initial yield stress in out-of-plane shear /MPa
42	B_τ	Hardening parameter for out-of-plane shear /MPa
43	C_τ	Hardening parameter for out-of-plane shear

Chapter 5

Simulations and results

In this chapter the behaviour of the proposed model is illustrated. The model is tested in one dimensional tests for each direction of the model. Furthermore, a more complex model is presented simulating creasing of paperboard. The parameters for the in-plane model are set according to Xia (2002) (cf. table 5.1) since the in-plane model is a small deformation version of this model. The in-plane model presented behaves in the same manner as the model proposed by Xia (2002) with the restriction for small deformations, and can be calibrated with the procedures presented in Nygårds (2005) and Ristinmaa (2003). The parameters for the out-of-plane compression is set to follow the behaviour of the model proposed by Stenberg (2003). The out-of-plane shear behaviour relevant to the continuum model has to the knowledge of the author not been experimentally examined and the calibration has been done with help of a creasing operation. It is outside the scope of this work to develop a procedure to calibrate the parameters for the out-of-plane model and the simulations are mainly done to see that the model works and show *if* the parameters can be set to capture the relevant behaviour. The parameters of the interface model is set according to Xia, cf. table 5.2.

5.1 Set-up in the simulations

The model for creasing and folding is built up in ABAQUS/CAE (Complete ABAQUS Environment) version 6.5 and the simulations are executed in ABAQUS/Standard version 6.4. The model can be seen in figure 5.1 and is built to replicate configuration 6 in the experimental tests performed by Elison and Hansson (2005). The thickness of the board is 0.46 mm and the different properties of the paperboard are applied according to figure 5.2. The creasing is done with the MD along the direction of the set up i.e. the crease is in the CD. The model is three dimensional but to reduce the computational cost of the simulations the width in CD is just 0.01 mm with symmetry-boundary conditions making the model 0.02 mm wide in CD. Hence, the model almost experiences plain stress state.

Table 5.1: Elastic and plastic material properties for the sample fiveply paperboard, numerical values for the chemical plies and the mechanical plies as reported by Xia (2002).

Prop.	Notation	Description	Chem.	Mech.
1	E_x	Elastic modulus in MD /MPa	8900	3400
3	E_y	Elastic modulus in CD /MPa	3400	960
4	ν_{xy}	In-plane Poisson's ratio	0.37	0.37
6	G_{xy}	In-plane shear modulus /MPa	2400	800
11	σ_1^0	Parameter for initial tensile yield plane in MD[a] /MPa	22.0	10.7
12	σ_2^0	Parameter for tensile yield plane in CD[b] /MPa	16.5	6.5
13	σ_3^0	141.4% of initial yield stress in pure shear /MPa	8.0	6.0
14	σ_4^0	Parameter for compression yield plane in MD[c] /MPa	6.3	6.3
15	σ_5^0	Parameter for compression yield plane in CD[d] /MPa	6.3	6.3
16	A_1	Hardening parameter /MPa	44.0	19.0
17	A_2	Hardening parameter /MPa	7.4	7.4
18	A_3	Hardening parameter /MPa	18.0	7.5
19	A_4	Hardening parameter /MPa	12.0	6.0
20	A_5	Hardening parameter /MPa	12.5	9.0
21	B_1	Hardening parameter	260.0	260.0
22	B_2	Hardening parameter	160.0	160.0
23	B_3	Hardening parameter	375.0	375.0
24	B_4	Hardening parameter	160.0	160.0
25	B_5	Hardening parameter	310.0	310.0
26	C_1	Hardening parameter /MPa	800.0	800.0
27	C_2	Hardening parameter /MPa	160.0	160.0
28	C_3	Hardening parameter /MPa	200.0	200.0
29	C_4	Hardening parameter /MPa	300.0	300.0
30	C_5	Hardening parameter /MPa	225.0	225.0
	2k	Exponent in yield condition	4	4
	$d\varepsilon_{MD}^p/d\varepsilon_{CD}^p$	Plastic strain ratio in MD	-0.5	-0.5
	$d\varepsilon_{CD}^p/d\varepsilon_{MD}^p$	Plastic strain ratio in CD	-0.133	-0.133
34	μ	Parameter for elastic behaviour in ZD	0.026	0.026
35	r_{orig}	Initial void ratio	1.12	1.12
36	σ_z^t	Strength in ZD tension /MPa	0.36	0.36
37	A_σ	Hardening parameter for ZD compression /MPa	0.4378	0.4378
38	B_σ	Hardening parameter for ZD compression /MPa	-1	-1
39	C_σ	Hardening parameter for ZD compression	6.5	6.5
40	$G_{xz} = G_{yz}$	Shear modulus in out-of-plane shear /MPa	400	400
41	A_τ	Initial yield stress in out-of-plane shear /MPa	5	5
42	B_τ	Hardening parameter for out-of-plane shear /MPa	3	3
43	C_τ	Hardening parameter for out-of-plane shear	2	2

[a] 91.0% of initial yield stress with present parameters for chemical ply
[b] 129.9% of initial yield stress with present parameters for chemical ply
[c] 89.4% of initial yield stress with present parameters for chemical ply
[d] 99.1% of initial yield stress with present parameters for chemical ply

Table 5.2: Model parameters needed in the interface model. Parameters have been reported by Xia (2002) for the outer and inner interfaces in a five-ply paperboard.

Prop		Definition	Outer	Inner
1	$K^0_{t_1}$	Initial stiffness in MD shear /(MPa/mm)	800	640
2	K^0_n	Initial stiffness in tension /(MPa/mm)	400	320
3	$S^0_{t_1}$	Initial yield stress in MD shear /MPa	1.45	1.18
4	S^0_n	Initial yield stress in tension /MPa	0.45	0.35
5	$K^0_{t_2}$	Initial stiffness in CD shear /(MPa/mm)	800	640
6	$S^0_{t_2}$	Initial yield stress in CD shear /MPa	1.45	1.18
7	A	Initial friction	0.28	0.28
8	B	Reductional friction	0.99	0.99
9	C	Initial plastic displacement (damage constant) /mm	0.085	0.085
10	R^s_n	ZD residual strength factor /MPa	0.97	0.97
11	$R^s_{t_1}$	MD shear residual strength factor /MPa	0.87	0.87
12	$R^s_{t_2}$	CD shear residual strength factor /MPa	0.87	0.87
13	R^k_n	ZD residual strength factor /MPa	0.97	0.97
14	$R^k_{t_1}$	MD shear residual strength factor /MPa	0.87	0.87
15	$R^k_{t_2}$	CD shear residual strength factor /MPa	0.87	0.87
-	A_1		9.0	9.0
-	B_1		140.0	140.0

Table 5.3: Components for the normals to the yield planes, $\boldsymbol{N}$.

α	$(N_{xx})_\alpha$	$(N_{yy})_\alpha$	$(N_{xy})_\alpha$	Yield plane
1	$2/\sqrt{5}$	$-1/\sqrt{5}$	0	MD tension
2	$-2/\sqrt{229}$	$15/\sqrt{229}$	0	CD tension
3	0	0	$1/\sqrt{2}$	Positive shear
4	$-2/\sqrt{5}$	$1/\sqrt{5}$	0	MD compression
5	$2/\sqrt{229}$	$-15/\sqrt{229}$	0	CD compression
6	0	0	$-1/\sqrt{2}$	Negative shear

The reaction force and the displacement of the male die is measured according to figure 5.3. In order to get comparable forces the reaction is multiplied with the width of the test piece. The specimens used in the experiments had the width 38±1mm. The shape of the male and female die is described in figure 5.4. A web tension of 1000 N/m was applied to the end of the paperboard and stoppers are located at the top of the paperboard according to figure 5.1. The stoppers where not included in the test equipment but was used in the model to keep the paperboard in place. The stoppers and male die are assumed to be frictionless and the female die is assumed to have the friction coefficient 0.1.

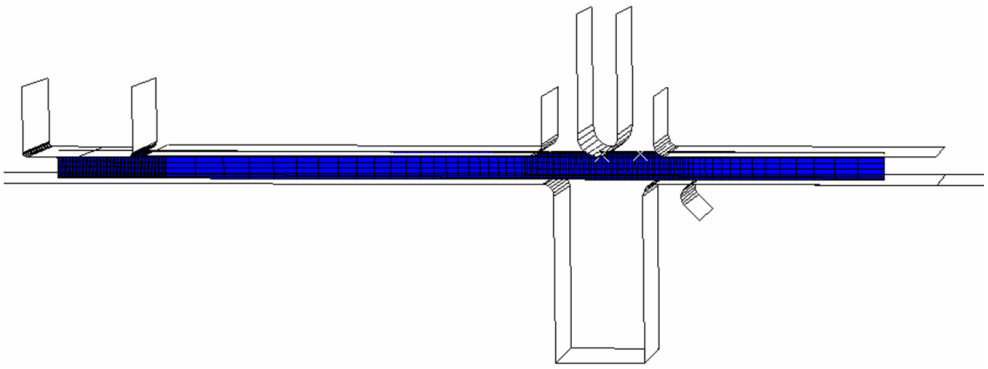

Figure 5.1: Set-up in the simulations.

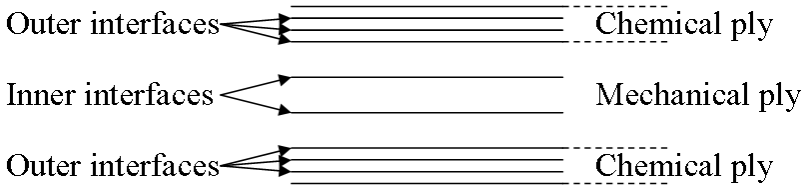

Figure 5.2: Material and interface properties.

5.2 Results

The simulations for the uniaxial tension and compression and pure shear, seen in figure 5.5 to 5.7, is done for one gauss point in CALFEM/MATLAB. The code is the same as in the UMAT with small changes to fit the different notations.

In figure 5.8 and 5.9 the simulation of the crease is seen. In figure 5.8 the male die is in its deepest position and 5.9 is from the end of the process. The colours represent the different values of the plastic strain in ZD compression.

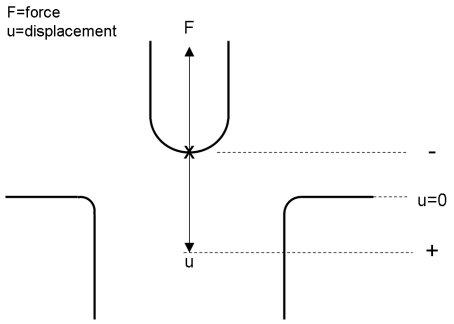

Figure 5.3: Definitions of the force acting on and displacements of the male die.

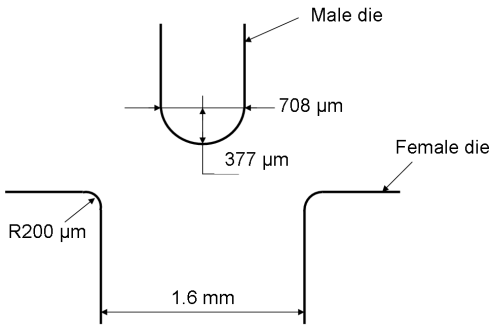

Figure 5.4: Measure of male- and female die in simulations.

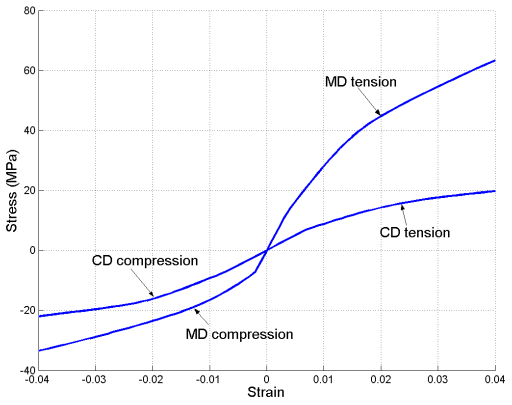

(a) Four different curves for uniaxial compression and tension.

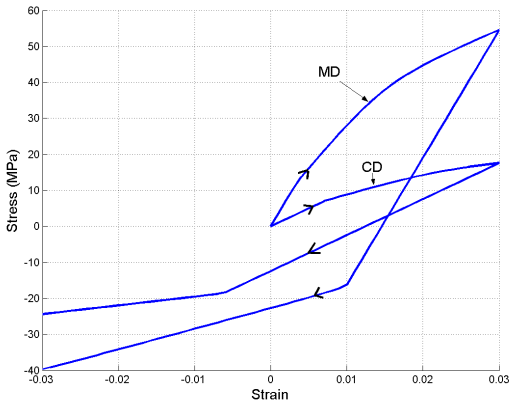

(b) Uniaxial tension and subsequent compression.

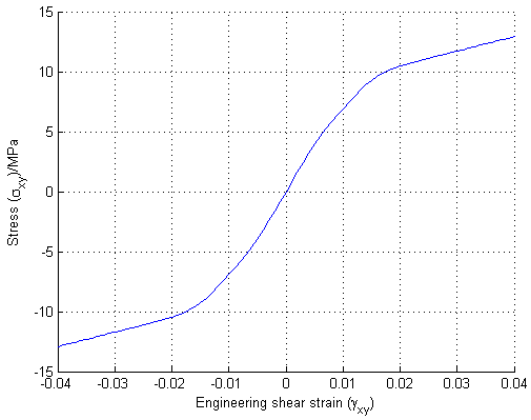

(c) Two different curves for positive and negative shear.

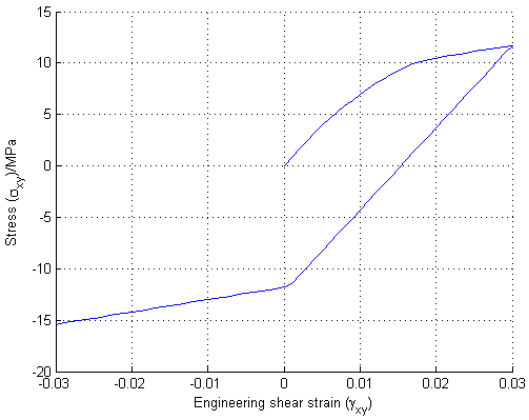

(d) Positive shear and subsequent negative shear.

Figure 5.5: Simulation of in-plane behaviour of mechanical plies of paperboard.

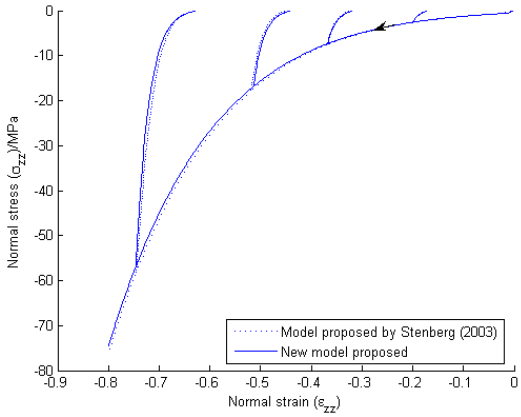

(a) ZD-compression in subsequent loading and unloading compared with model by Stenberg (2003).

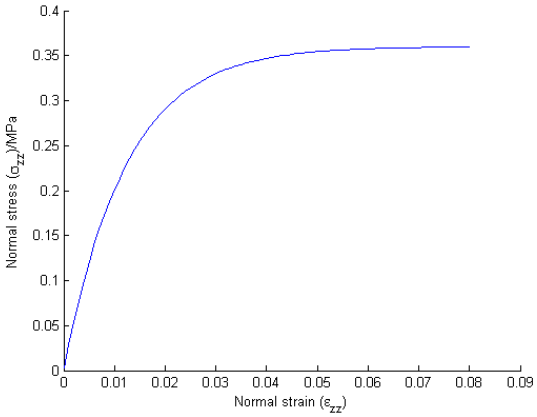

(b) ZD-tension. Has only elastic behaviour.

Figure 5.6: Out-of-plane normal behaviour of continuum model.

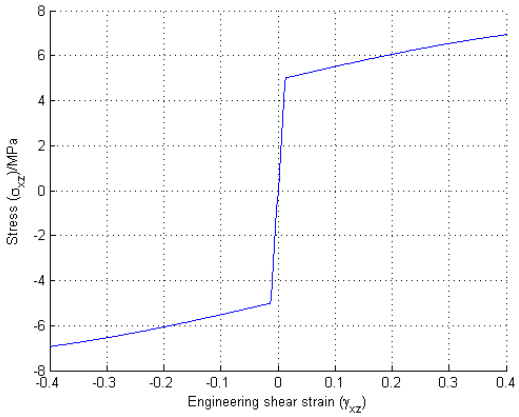

(a) Two different curves for positive and negative shear.

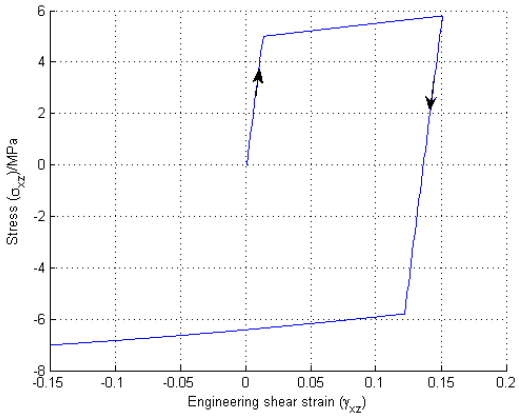

(b) Positive shear and subsequent negative shear.

Figure 5.7: Out-of-plane shear behaviour of continuum model.

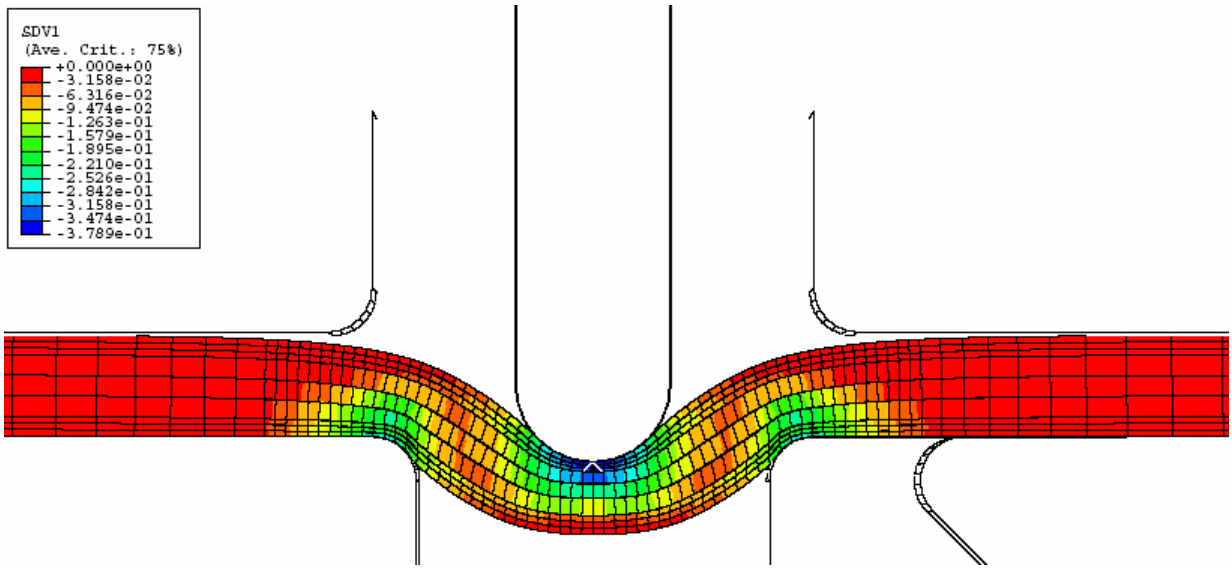

Figure 5.8: Simulation of creasing of paperboard with male die in its deepest position.

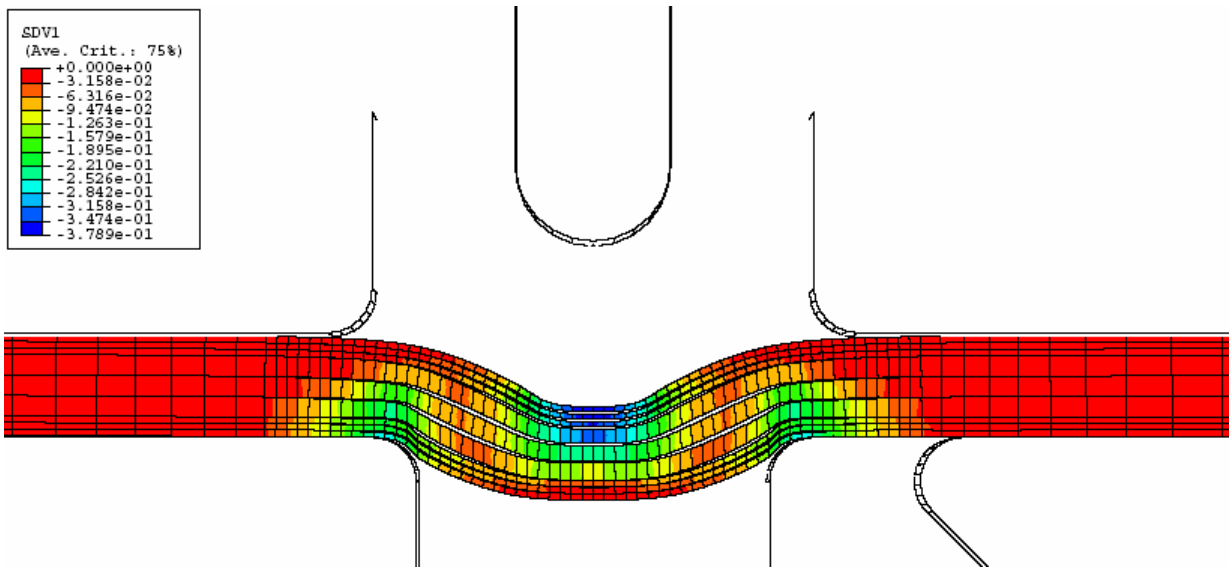

Figure 5.9: Simulation of creasing of paperboard; end of procedure.

Figure 5.10 shows the force-displacement curves for the male die. The different curves represent experiment, simulation with the 3DM model with parameters from Xia (2002), simulation with the 3DM model with parameters from Nygårds (2005) and simulation with the model proposed in this thesis. The experimental data and the simulation with the parameters from Xia (2002) is obtained from Elison and Hansson (2005). The simulation set-up is the same in the simulation by Nygårds (2005) and for the simulation with the proposed model. It is a slight difference between this set-up and the simulation set-up used by Elison and Hansson (2005). Both set-ups are however built to resemble the experimental set-up.

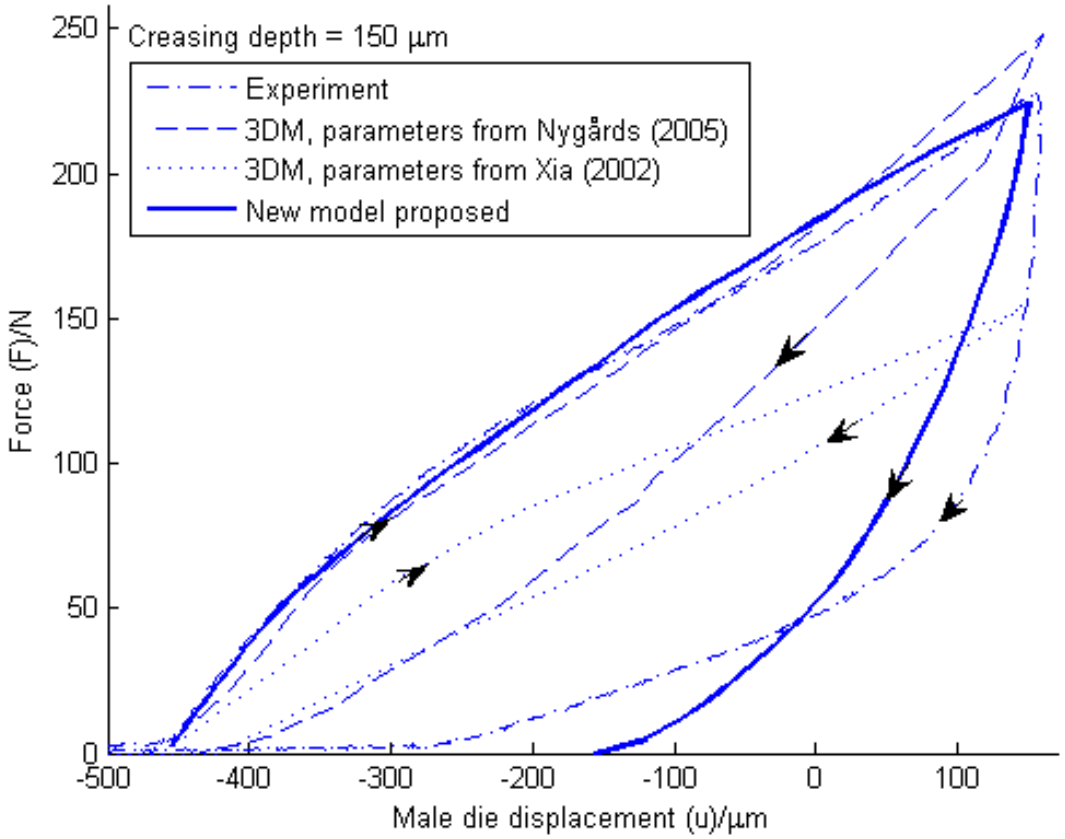

Figure 5.10: Force-displacement diagram for the male die in creasing.

Chapter 6

Discussion and conclusions

In figure 5.10 the result of the simulations is seen. The behaviour in unloading is better than for the original 3DM model. The out-of-plane shear parameters can be set to better capture the initial part of the unloading but will then not give the accurate remaining deformation, or the parameters can be set to give the accurate remaining deformation but the unloading curve will then not be accurate. In other words the stiffness change during unloading in the experiments seen in figure 5.10 can not be captured. From the results presented in figure 5.10 it can seem as if we get very good results, but it should be remembered that the out-of-plane shear components has not been experimentally determined, and we have freedom to set these in order to capture the creasing procedure.

An advantage with the implementation of the proposed model is that the tolerance criteria set by ABAQUS/Standard does not have to be changed due to convergence problems as has been reported for the present implementation of the 3DM model (Elison and Hansson, 2005). By not increasing these parameters causes the simulation curve to be smoother and more accurate than if the parameters are changed. That the implementation of the proposed model gives a smoother curve than for the present implementation of the 3DM model can be seen in figure 5.10.

The most important note to make about the model proposed is that it is a small deformation model. The model does not make a difference between the deformed configuration and the original configuration, it solves the equations in the original configuration without mapping the forces between the two states. This has the effect that the rigid body rotation in the creasing procedure will cause stress in the paper. It is outside the scope of this work to incorporate large rotations, but it is believed that this can be done with (hopefully) relatively small efforts by letting the FE-software use co-rotated strains and stresses.

The three dimensional small deformation continuum model presented is this thesis is split into two uncoupled models; the in-plane model and the out-of-plane model. To do this, two assumptions has to be made. First, the two Poisson's ratios coupled to the through-thickness directions are assumed to be zero, according to many investigations this does not

seem to be far from the truth. Secondly, the in-plane behaviour is assumed not to depend on the out-of-plane deformations and vice versa. The second assumption is not evident and it would to some extent be surprising if it holds, especially the high compressions that a creasing procedure causes could probably affect the in-plane behaviour.

As mentioned in a previous chapter the set-up is built up in a way that lets the paper almost experience plain stress state. However, it would probably have been better to apply plain strain state to the paperboard or increase the width of the paperboard in the model to get a simulation set-up with more close correlation to the experiments.

In a creasing procedure the three important components are the normal behaviour in ZD, one in-plane direction and the shear between these two directions. The continuum model proposed by Xia (2002) has plasticity in the in-plane direction and only elasticity in the two remaining components. The interface model proposed by Xia (2002) separates the layers of elements and incorporates remaining stresses between the layers and it can be argued that this will lead to remaining plasticity in the paperboard. However, this has been examined by Elison and Hansson (2005) and as can be seen in figure 5.10 this does not lead to enough deformation after a crease. Therefore it is believed that a model, as the one presented in this thesis, with plasticity in all components is important.

6.1 Further work

As mentioned earlier it is seen in figure 5.10 that the experiments during unloading has a stiffness change i.e. an angle that can not be captured with the present model. One reason for this could be that the elastic out-of-plane shear stiffness depends on the ZD compression. To visualize this check figure 6.1. It could be that the paper in figure 6.1(b) is harder to shear, in order to give the same shear strain as in figure 6.1(a), since the fibres are more closely packed. If this holds it should be noted that it is not strictly true to refer to paper as an orthotropic material since, as can be seen in equation 3.6, there is no coupling between normal strain and shear stress in orthotropic materials.

As mentioned in the previous section the in-plane model and the out-of-plane model are uncoupled. To fully examine this coupling in order to get the full yield surface, and the evolvement of it, for all components in the continuum model is very hard to do, but to strive to do this would give much knowledge in order to build an accurate material model.

Elison and Hansson (2005) has shown in a parameter study that the interface parameters are ”very important” in the original 3DM model, and that even small changes of the interface parameters affect the result. It is believed that the interface model is as important in the proposed model as in the original 3DM model for the creasing operation. Not as important as the relevant components in the continuum model but still important. Therefore, it is of vital importance to calibrate the out-of-plane model in the continuum model together with the interface model so that they together capture the relevant behaviour. It should also be

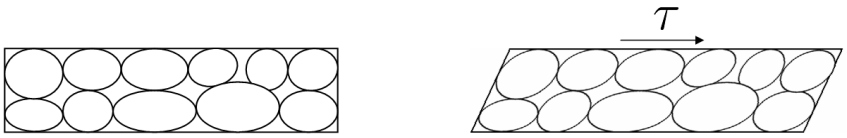

(a) Schematic of uncompressed fibres.

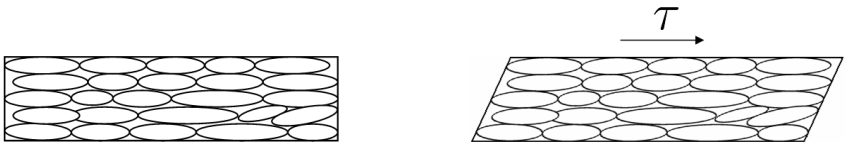

(b) Schematic of compressed fibres.

Figure 6.1: The effect that compressed fibers could have a larger shear stiffness than uncompressed fibres is not incorporated in the proposed model or in any orthotropic material.

noted that since the interface model is a traction-displacement based model the number of interfaces used in the simulations is important to consider when the models are calibrated.

It is, as mentioned earlier, important to add a model that controls the delamination since only one continuum model can not capture this behaviour, but since the interface model only incorporates remaining stresses and separate the plies this may not damage the structure enough during a creasing operation, to give the proper behaviour in the subsequent folding. *If* it is shown that the structural weakening due to the separation of the plies is not enough in the present models, one way of handling this could be to let the model that controls the delamination have a distribution in ZD according to figure 6.2. When the delamination model weakens in the plastic region the elements will not be able to take up load and the structure softens. This can be seen as the fibres that take part of the delamination process and are unable to take up a substantial amount of load.

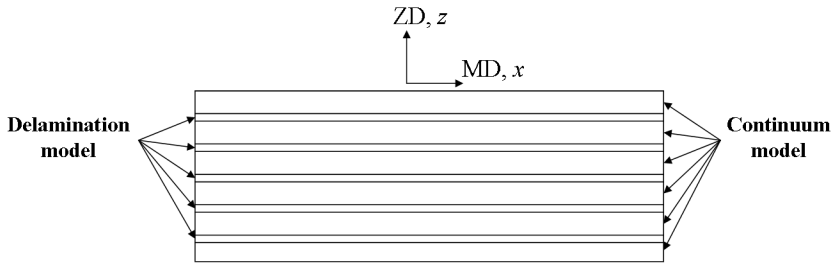

Figure 6.2: Proposal for a delamination model with distribution in ZD.

The in-plane model has isotropic hardening, i.e. it makes no difference between different types of plastic strain. *If* experiments show that this does not hold, use can be made of the fact that the model is made up of several yield planes. Therefore, we can - instead of adding kinematic or mixed hardening - couple extra plastic variables which evolve with

and control the different yield planes.

In the in-plane model it is assumed that the flow is associated and in order to get the plastic strain ratios correct ($\frac{d\varepsilon^p_{CD}}{d\varepsilon_{MD}}$ for MD tension and $\frac{d\varepsilon^p_{MD}}{d\varepsilon_{CD}}$ for CD tension) the shape of the yield surface is changed. This coupling between the shape of the yield surface and the flow direction is not evident. And it is proposed that the experiments measured for the biaxial failure surfaces are better as a ground for the shape of the yield surface than the plastic strain ratios. However, in order to uncouple the flow direction and the plastic strain ratios from the shape of the yield surface a non-associate flow rule is required.

The present in-plane model relies on the assumption that the yield surface has the same characteristics as the, in experiments observed, failure surface. This is done since no yield surface for paper has been measured. Since the yield surface and the evolvement of it forms the ground in material models the biaxial yield surface for paper would be valuable to examine.

During this work data for the out-of-plane compression of paperboard was unavailable. Instead, the behaviour of the out-of-plane model in compression was fitted to the model presented by Stenberg (2003). The proposed model should be calibrated to fit experimental data.

Both the present implementation of the 3DM model Nygårds (2005) and the model presented in this thesis make use of fact that the theory presented by Xia (2002) has a symmetric stress and strain tensor. This together with the fact that only three components are present in the in-plane model results in that we can use a vector with three components and engineering shear strain instead of the full second order tensor for the stress and strain. This way the implementation becomes easier. However, in the implementation an extra factor 2 is required when summation convention is used. If instead the definitions are changed to fit with engineering sheer strain and that the effective plastic strain is defined as $\varepsilon^p_{eff} = \|\varepsilon^p_i\|$ this would have the advantages that; the implementation would be more straight forward; the flow direction $\boldsymbol{N}$ could be normalized towards pure engineering shear stress at the same time as the parameters for the yield planes for shear, σ^{III}_s, (S^{III} for large deformations) take the same values as the yield stress in pure shear; the interpretation of the pure shear behaviour would fit to the use of engineering shear strain. This would however be a change in the formulation of the theory and calibration of the shear components would have to be remade.

Additionally, a few other extensions can be added to incorporate other behaviour of the paperboard.

- Fracture conditions.
- Strain rate effects, this opens up for the possibility to predict creep.
- Moisture dependence

Bibliography

ABAQUS (2004). *ABAQUS User's Manual*. Hibbitt, Karlsson & Sorensen Inc, Pawtucket, RI, USA, 6.5 edition.

Arcan, M., Hashin, Z., and Voloshin, A. (1978). A method to produce uniform plane-stress states with application to fiber-reinforced materials. *Experimental Mechanics*, 18(4):141–146.

Austrell, P. E., Dahlbom, O., Lindeman, J., Olsson, A., Olsson, K., Persson, K., Petersson, H., Ristinmaa, M., Sandberg, G., and Wernberg, P. A. (2004). *CALFEM - A Finite Element toolbox*. The division of structural mechanics, Lund University, 3.4 edition.

Baumgarten, H. L. and Göttsching, L. (1973). Triaxial deformation of paper under tensile loading. In *Proc. The fundamental properties of paper related to its uses*, pages 227–249, Cambridge, England. The Brittish paper and board industry federation.

Belytschko, T., Liu, W. K., and Moran, B. (2000). *Nonlinear finite elements for continua and structures*. John Wiley & Sons Ltd.

Carlsson, L., Ruvo, A. D., and Fellers, C. (1983). Bending properties of creased zones of paperboard related to interlaminar defects. *Journal of Materials Science*, 18:1365–1373.

deRuvo, A., Carlsson, L., and Fellers, C. (1980). The biaxial strength of paper. *TAPPI*, 63:133–136.

Dunn, H. M. (2000). Micromechanics of paperboard deformation. Master's thesis, Massachusetts institute of technology.

Elison, O. and Hansson, L. (2005). Evaluating the 3DM model - An experimental and finite element study. Master's thesis, Department of mechanical engineering, Solid mechanics, Lund institute of technology.

Fellers, C. and Norman, B. (1998). *Pappersteknik*. Institutionen för Pappersteknik, Kungl Tekniska Högskolan, Stockholm, third edition.

Fellers, C., Westerlind, B., and deRuvo, A. (1981). An investigation of the biaxial failure envelope of paper. *Proceeding of 7th Fundamental Research Symposium: The Role of Fundamental Research in Papermaking*, pages 527–556.

Gunderson, D. E. (1983). Determining paperboard strength. *International Paper Physics Conference*, pages 253–263.

Hill, R. (1950). *The mathematical theory of plasticity*. Clarendon Press, Oxford.

Öhrn, O. E. (1965). Thickness variations of paper on stretching. *Svensk Papperstidning*, 68(5):141–149.

Lagace, P. A. (2005). *Equations of elasticity*. Massachusetts Institute of Technology, OpenCourseWare (http://ocw.mit.edu/NR/rdonlyres/Aeronautics-and-Astronautics/16-20Structural-MechanicsFall2002/891F16EA-EA88-4250-8AE5-1B3D6BA12511/0/unit4.pdf), 12/12 2005.

Mahnken, R. (1999). Aspects on the finite-element implementation of the gurson model including parameter identification. *International Journal of Plasticity*, 15:1111–1137.

Mann, R., Baum, G., and Habeger, C. (1980). Determination of all nine orthotropic elastic constants for machine-made paper. *Tappi Journal*, 63(2):163–166.

Nygårds, M. (2005). 3DM - Three dimensional finite element modelling of paperboard. Technical Report no. 67, STFI-Packforsk.

Ortiz, M. and Popov, E. (1985). Accuracy and stability of integration algorithms for elastoplastic constitutive equations. *International Journal for Numerical Methods in Engineering*, 21:1561–1576.

Ottosen, N. and Petersson, H. (1992). *Introduction to the Finite Element Method*. Prentice Hall.

Ottosen, N. and Ristinmaa, M. (2005). *The Mechanics of Constitutive Modeling*. Elsevier, first edition.

Persson, K. (1991). Material model for paper. Master's thesis, Lund institute of Technology, Lund, Sweden.

Ristinmaa, M. (2003). Review of plasticity model for paper and paperboard. Technical report, Division of Solid Mechanics, Lund University.

Stenberg, N. (2002a). *On the out-of-plane mechanical behaviour of paper materials*. PhD thesis, Royal Institute of Technology (KTH), Solid Mechanics.

Stenberg, N. (2002b). Out-of-plane shear of paperboard under high compressive loads. *Journal of Pulp and Paper Science*, 30(1):22–28.

Stenberg, N. (2003). A model for the through-thickness elastic-plastic behaviour of paper. *International Journal of Solids and Structures*, 40:7483–7498.

Stenberg, N. and Fellers, C. (2002). The out-of-plane poisson's ratios of paper and paperboard. *Nordic Pulp and Paper Research Journal*, 17(4):387–394.

Stenberg, N., Fellers, C., and Östlund, S. (2001a). Measuring the stress-strain properties of paperboard in the thickness direction. *Journal of pulp and paper science*, 27(6):213–221.

Stenberg, N., Fellers, C., and Östlund, S. (2001b). Plasticity in the thickness direction of paperboard under combined shear and normal loading. *Journal of Engineering Materials and Technology*, 123:184–190.

Tsai, S. and Wu, E. (1971). A general theory of strength for anisotropic materials. *Journal of Composite materials*, 5:58–80.

Xia, Q. S. (2002). *Mechanics of inelastic deformation and delamination in paperboard*. PhD thesis, Massachusetts institute of technology.

Zienkiewicz, O. C. and Taylor, R. L. (2000). *The finite element method*. Butterworth-Heinemann, fifth edition.

Appendix A

Comments to the model proposed by Stenberg (2003)

It has been inside the scope of this master's thesis to incorporate a model for the out-of-plane behaviour of the continuum model. A model formulated by Stenberg (2003) was first implemented, but two problems occurred that made the model unsuitable. Therefore, a new model has been developed and reported in this work. In this appendix the problems with the model by Stenberg (2003) are described. Since another model is proposed in this report we will not go into details on the model, for further details cf. Stenberg (2003).

A.1 ZD compression

In this section the ZD compression of the model is reviewed. In the plastic region this model has two different solutions. One correct that follows the desired curve and one where the solution takes a wrong curve and the increment of the plastic multiplier ($\Delta\lambda$) takes negative values. The second solution is therefore clearly wrong. To have two different solutions where one is wrong is not unusual in numerical analysis and sometimes occur in numerical methods within constitutive modelling, reported before by Mahnken (1999). The problem in this model is instead that there is a jump for the right solution when going from the elastic to the plastic region as can be seen in figure A.1. This causes considerable problems when solving it numerically (and it is not the way the material would act). In figure A.1 this behaviour is illustrated.

To further visualize this problem cf. figure A.2. Since we have implicit equations both for the elastic region and the plastic region, the problem is solved numerically. The solution procedure is set up in the same manner as earlier with the solution reached when a function, F, reaches zero. This function is plotted in figure A.2 at the position when the solution goes from elastic to plastic response. We here see the two solutions for the plastic function

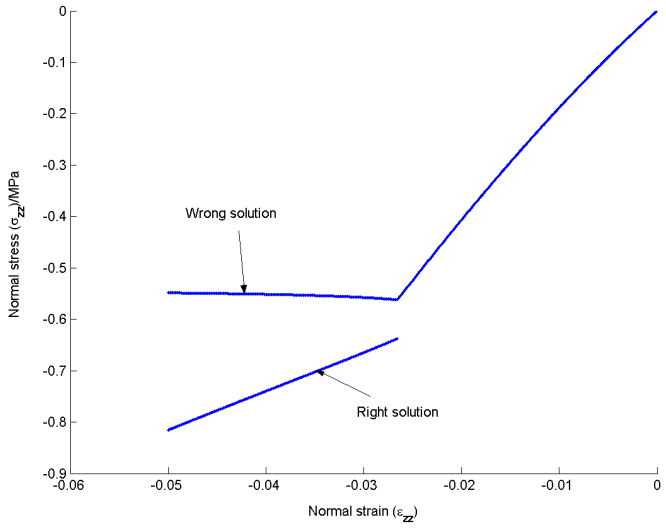

Figure A.1: ZD-compression in model proposed by Stenberg (2003).

where one coincides with the elastic function.

A.2 Shear model

Stenberg has measured the yield surface in a modified Arcan device (Stenberg et al., 2001b) and sheared it along the fibres according to figure A.3. The delamination between the fibres has been measured and this shear behaviour is not suitable for the continuum model that is supposed to capture the behaviour of the fibres. Figure A.4 shows the beginning of plasticity in the out-of-plane shear components, with the different colours representing the out-of-plane shear stress. The hardening is described by a hyperbolic tangent-function that reaches a plateau. The material can not take up more shear force when the top load is reached and the material deforms with ideal-plasticity, cf. figure A.5. The shear model proposed by Stenberg (2003) is to some extent a delamination model.

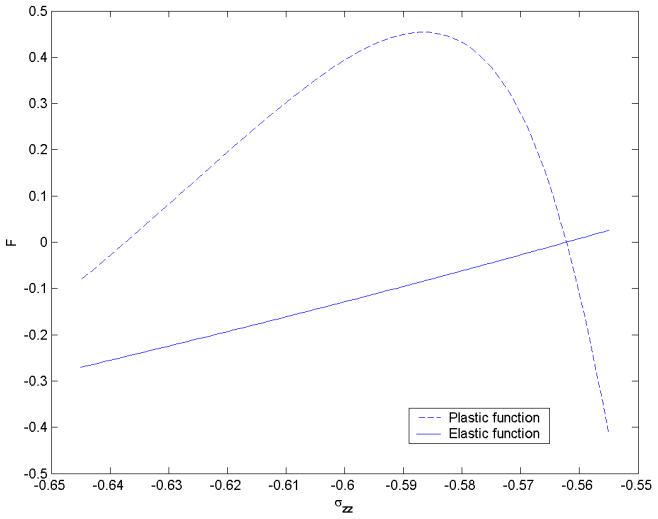

Figure A.2: The functions to solve for the plastic solution and the elastic solution in the boundary between plastic and elastic region.

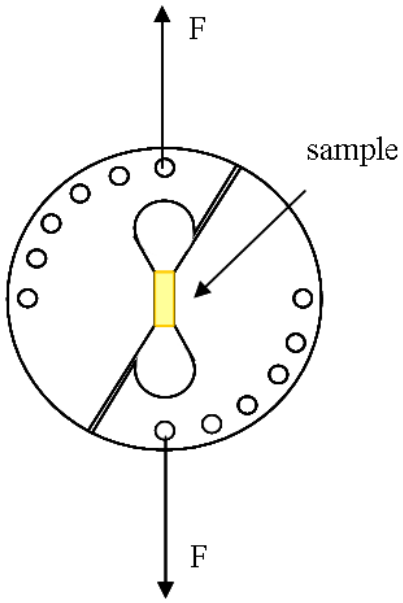

Figure A.3: Principle of device used in measuring the out-of-plane shear behaviour.

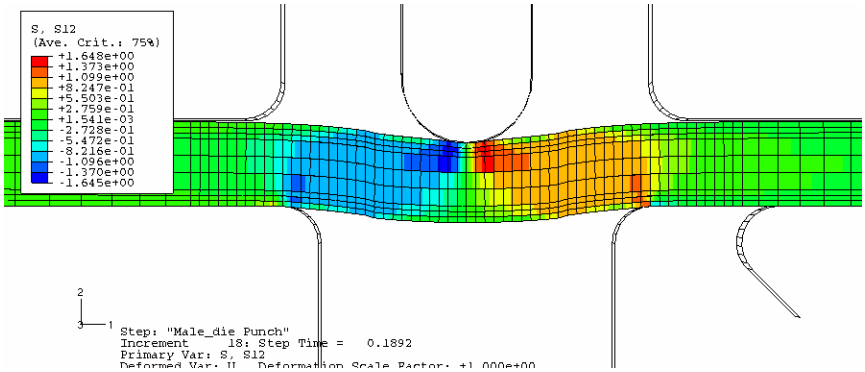

Figure A.4: Beginning of plastic shear deformation in out-of-plane shear model proposed by Stenberg (2003).

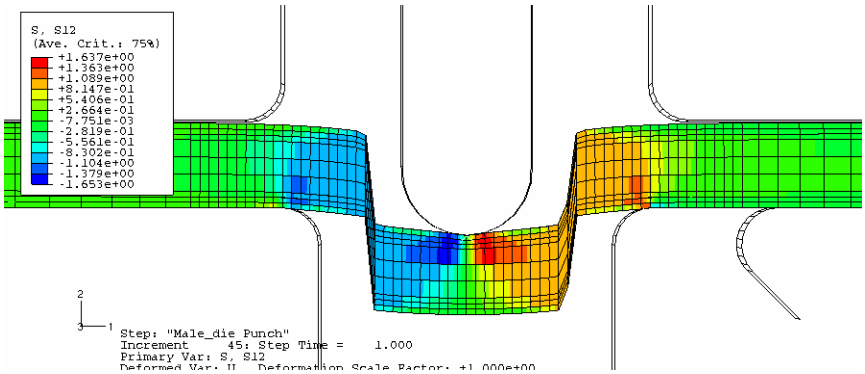

Figure A.5: End of creasing in out-of-plane shear model proposed by Stenberg (2003).

Appendix B

Calculations used in the implementation

B.1 In-plane model

In order to calculate the stress we need to solve equation (4.14) that for the in-plane model takes the form

$$\boldsymbol{\mathcal{F}} = \begin{bmatrix} \sigma_{xx}^{(i)} - \sigma_{xx}^{\star} + D_{1k}\Delta\lambda K_k^{(i)} \\ \sigma_{yy}^{(i)} - \sigma_{yy}^{\star} + D_{2k}\Delta\lambda K_k^{(i)} \\ \sigma_{xy}^{(i)} - \sigma_{xy}^{\star} + D_{3k}\Delta\lambda K_k^{(i)} \\ \sum_{I=1}^{n} \chi_I \left(\frac{\boldsymbol{\sigma}_i^{(i)} \boldsymbol{N}_i^I}{\boldsymbol{\sigma}_s^{I(i)}} \right)^{2k} - 1 \end{bmatrix} = \boldsymbol{0}. \tag{B.1}$$

With the unknowns

$$\boldsymbol{x} = \begin{bmatrix} \Delta\lambda \\ \sigma_{xx}^{(i)} \\ \sigma_{yy}^{(i)} \\ \sigma_{xy}^{(i)} \end{bmatrix}. \tag{B.2}$$

A factor 2 is required for the shear components due to the summation convention, this is for convenience added in the vector $\boldsymbol{N}$, hence

$$\boldsymbol{N} = \begin{bmatrix} N_{xx} \\ N_{yy} \\ 2N_{xy} \end{bmatrix}. \tag{B.3}$$

Equation (B.1) is solved with the Newton-Raphson procedure described in equation (4.18). With the Jacobian

$$\frac{d\boldsymbol{\mathcal{F}}}{dx} = \begin{pmatrix} \frac{\partial \mathcal{F}_1}{\partial x_1} & \frac{\partial \mathcal{F}_1}{\partial x_2} & \frac{\partial \mathcal{F}_1}{\partial x_3} & \frac{\partial \mathcal{F}_1}{\partial x_4} \\ \frac{\partial \mathcal{F}_2}{\partial x_1} & . & . & . \\ \frac{\partial \mathcal{F}_3}{\partial x_1} & . & . & . \\ \frac{\partial \mathcal{F}_4}{\partial x_1} & . & . & . \end{pmatrix}, \tag{B.4}$$

where the components are

$$\frac{\partial \mathcal{F}_i}{\partial x_1} = D_{ik}(K_k + \Delta\lambda \frac{\partial K_k}{\partial \hat{K}_l} \frac{\partial \hat{K}_l}{\partial \Delta\lambda}), \tag{B.5}$$

$$\frac{\partial \mathcal{F}_i}{\partial x_{j+1}} = \delta_{ij} + D_{ik}\Delta\lambda(2k-1)(2k) \sum_{I=1}^{n} \left(\frac{\sigma : \mathbf{N}_I}{\sigma_s^I} \right)^{2k-2} \chi_I \frac{\mathbf{N}_k^I}{(\sigma_s^I)^2} N_j^I, \tag{B.6}$$

$$\frac{\partial \mathcal{F}_4}{\partial x_{i+1}} = \hat{K}_i \tag{B.7}$$

and

$$\frac{\partial \mathcal{F}_4}{\partial x_1} = -2k \sum_{I=1}^{n} \left[\frac{(\sigma : \mathbf{N}_I)^{2k}}{(\sigma_s^I)^{2k+1}} \chi_I \left(A_I B_I tanh^2(B_I(\Delta\lambda + \varepsilon^{p(n)})) + C_I \right) \right]. \tag{B.8}$$

These components contains

$$\hat{K}_i = 2k \sum_{I=1}^{n} \left(\frac{\sigma : \mathbf{N}_I}{\sigma_s^I} \right)^{2k-1} \chi_I \frac{\mathbf{N}_i^I}{\sigma_s^I} \tag{B.9}$$

$$, \tag{B.10}$$

$$\frac{\partial K_k}{\partial \hat{K}_l} = \frac{1}{(\hat{K}_1^2 + \hat{K}_2^2 + \hat{K}_3^2)^{3/2}} \begin{pmatrix} \hat{K}_2^2 + \hat{K}_3^2 & -\hat{K}_1\hat{K}_2 & -\hat{K}_1\hat{K}_3 \\ -\hat{K}_1\hat{K}_2 & \hat{K}_1^2 + \hat{K}_3^2 & -\hat{K}_2\hat{K}_3 \\ -\hat{K}_1\hat{K}_3 & -\hat{K}_2\hat{K}_3 & \hat{K}_1^2 + \hat{K}_2^2 \end{pmatrix}, \tag{B.11}$$

$$\frac{\partial \hat{K}_k}{\partial \Delta\lambda} = -2k * 2k \sum_{I=1}^{n} \frac{(\sigma : \mathbf{N}_I)^{2k-1}}{(\sigma_s^I)^{2k+1}} \chi_I \mathbf{N}_k^I \frac{\partial \sigma_s^I}{\partial \Delta\lambda} \tag{B.12}$$

and

$$\frac{\partial \sigma_s^\alpha}{\partial \Delta\lambda} = A_\alpha B_\alpha tanh^2(B_\alpha(\Delta\lambda + \varepsilon^{p(n)})) + C_\alpha. \tag{B.13}$$

In order to use the Newton-Raphson method a start guess is required. The start guess does not influence the result (if obtained), only the number of iterations required to achieve convergence. The start guess is taken as

$$\boldsymbol{x} = \begin{bmatrix} 0 \\ \sigma_{xx}^\star \\ \sigma_{yy}^\star \\ \sigma_{xy}^\star \end{bmatrix}. \tag{B.14}$$

B.1.1 Material tangent stiffness components

In order to calculate the consistent material tangent stiffness the following matrix is required

$$\frac{\partial \boldsymbol{\mathcal{F}}}{\partial \boldsymbol{\varepsilon}} = - \begin{pmatrix} D_{11} & D_{12} & D_{13} \\ D_{21} & D_{22} & D_{23} \\ D_{31} & D_{32} & D_{33} \\ 0 & 0 & 0 \end{pmatrix}. \tag{B.15}$$

B.2 Out-of-plane normal model

The elastic behaviour is described by the explicit equation

$$\sigma_{zz} = \sigma_z^t \left(1 - exp \left[\frac{1 + r_{orig}}{\mu} (exp[\varepsilon_{zz}^p] - exp[\varepsilon_{zz}]) \right] \right). \tag{B.16}$$

The plasticity is described by

$$\boldsymbol{\mathcal{F}} = \begin{bmatrix} \sigma_{zz} - \sigma_z^t \left(1 - exp \left[\frac{1+r_{orig}}{\mu} (exp[\varepsilon_{zz}^p - \Delta\lambda] - exp[\varepsilon_{zz}]) \right] \right) = 0 \\ \sigma_a(\Delta\lambda) - \sigma = 0 \end{bmatrix}. \tag{B.17}$$

The unknowns are

$$\boldsymbol{x} = \begin{bmatrix} \sigma_{zz} \\ \Delta\lambda \end{bmatrix}. \tag{B.18}$$

The required jacobian $\frac{d\boldsymbol{\mathcal{F}}}{d\boldsymbol{x}}$ has the components

$$\frac{\partial \mathcal{F}_1}{\partial x_1} = 1, \tag{B.19}$$

$$\frac{\partial \mathcal{F}_2}{\partial x_1} = -1, \tag{B.20}$$

$$\frac{\partial \mathcal{F}_2}{\partial x_2} = B_\sigma C_\sigma exp[-C_\sigma(\varepsilon_{zz}^p - \Delta\lambda)], \tag{B.21}$$

and

$$\frac{\partial \mathcal{F}_1}{\partial x_2} = -\sigma_z^t \frac{r_{orig} + 1}{\mu} \left(1 - exp \left[\frac{1 + r_{orig}}{\mu} (exp[\varepsilon_{zz}^p - \Delta\lambda] - exp[\varepsilon_{zz}]) + (\varepsilon_{zz}^p - \Delta\lambda) \right] \right). \tag{B.22}$$

Since the model only contains one component and that if plasticity occurs it will occur in that component, it is believed that it is a better assumption, for the start guess, that the entire step is plastic and the start guess is taken as

$$\boldsymbol{x} = \begin{bmatrix} \sigma_{zz}^\star \\ \Delta\varepsilon_{zz} \end{bmatrix}. \tag{B.23}$$

B.2.1 Material tangent stiffness components

The required matrix is

$$\frac{\partial \boldsymbol{\mathcal{F}}}{\partial \varepsilon_{zz}} = \begin{bmatrix} -\sigma_z^t \frac{r_{orig}+1}{\mu} exp\left[\frac{1+r_{orig}}{\mu}\left(exp[\varepsilon_{zz}^p - \Delta\lambda] - exp[\varepsilon_{zz}]\right) + \varepsilon_{zz}\right] \\ 0 \end{bmatrix}. \tag{B.24}$$

B.3 Out-of-plane shear model

It should be noted that the components presented in this section is not used in the UMAT, instead a more complex way is used to implement the shear components, but it is (strongly) believed that they give the same result and that the presented components would have given a simpler implementation.

In this section the subscript i, j, k and l takes the 1 (corresponding to xz) and 2 (corresponding to yz). For the out of plane shear components the system to solve is

$$\boldsymbol{\mathcal{F}} = \begin{bmatrix} \sigma_{xz}^{(i)} - \sigma_{xz}^{\star} + D_{1k}\Delta\lambda K_k^{(i)} \\ \sigma_{yz}^{(i)} - \sigma_{yz}^{\star} + D_{2k}\Delta\lambda K_k^{(i)} \\ \sqrt{\sigma_{xz}^2 + \sigma_{xz}^2} - \tau_s(\Delta\lambda) \end{bmatrix} = \mathbf{0}, \tag{B.25}$$

where

$$K_k^{(i)} = \frac{\frac{\partial f}{\partial \boldsymbol{\sigma}}}{\left\|\frac{\partial f}{\partial \boldsymbol{\sigma}}\right\|} \tag{B.26}$$

and

$$\frac{\partial f}{\partial \sigma_k} = \frac{\sigma_k}{\|\boldsymbol{\sigma}\|}. \tag{B.27}$$

The unknowns are

$$\boldsymbol{x} = \begin{bmatrix} \Delta\lambda \\ \sigma_{xz}^{(i)} \\ \sigma_{yz}^{(i)} \end{bmatrix}. \tag{B.28}$$

The required Jacobian has the components

$$\frac{\partial \mathcal{F}_i}{\partial x_1} = D_{ik}K_k, \tag{B.29}$$

$$\frac{\partial \mathcal{F}_3}{\partial x_1} = -B_\tau C_\tau tanh^2(C_\tau(\gamma_{eff}^p + x_1)), \tag{B.30}$$

$$\frac{\mathcal{F}_3}{x_{i+1}} = \hat{K}_i \tag{B.31}$$

and

$$\frac{\partial \mathcal{F}_i}{\partial x_{i+1}} = \delta_{ij} + D_{ik}\Delta\lambda \frac{\partial K_k}{\partial \hat{K}_l}\frac{\partial \hat{K}_l}{\partial x_{i+1}}. \tag{B.32}$$

With

$$\frac{\partial K_k}{\partial \hat{K}_l} = \frac{1}{(\hat{K}_1^2 + \hat{K}_2^2)^{3/2}} \begin{pmatrix} \hat{K}_2^2 & -\hat{K}_1\hat{K}_2 \\ -\hat{K}_1\hat{K}_2 & \hat{K}_1^2 \end{pmatrix} \tag{B.33}$$

and

$$\frac{\partial \hat{K}_l}{\partial x_{i+1}} = \frac{1}{(\sigma_1^2 + \sigma_2^2)^{3/2}} \begin{pmatrix} \sigma_2^2 & -\sigma_1\sigma_2 \\ -\sigma_1\sigma_2 & \sigma_1^2 \end{pmatrix}. \tag{B.34}$$

The start guess is taken as

$$\boldsymbol{x} = \begin{bmatrix} 0 \\ \sigma_{xz}^\star \\ \sigma_{yz}^\star \end{bmatrix}. \tag{B.35}$$

B.3.1 Material tangent stiffness components

The required matrix is

$$\frac{\partial \boldsymbol{\mathcal{F}}}{\partial \boldsymbol{\varepsilon}} = -\begin{bmatrix} G_{xz} & 0 \\ 0 & G_{yz} \end{bmatrix}. \tag{B.36}$$